LABORATORI NAZIONALI DI FRASCATI
SIS – Pubblicazioni

LNF–95/038 (P)
20 Luglio 1995

Calculation of the TeV Prompt Muon Component in Very High Energy Cosmic Ray Showers

G. Battistoni[1], C. Bloise[2], C. Forti[2]
M. Greco[2,3], J. Ranft[4] and A. Tanzini[5]
[1] *INFN, Sezione di Milano, Italy*
[2] *INFN, Laboratori Nazionali di Frascati, Italy*
[3] *Dipartimento di Fisica della III Università di Roma, Italy*
[4] *LAPP, Annecy–le–Vieux, France*
[5] *Dipartimento di Fisica della II Università di Roma, Italy*

ABSTRACT. HEMAS-DPM is a Monte Carlo for the simulation of very high energy cosmic ray showers, which includes the DPMJET–II code based on the two component Dual Parton Model. DPMJET–II provides also charm production in agreement with data and, for $p_\perp$ exceeding 5 GeV/c, with perturbative QCD results in hadron-nucleus and nucleus-nucleus interactions. In this respect, a new scheme has been considered for the inclusive production of D mesons at large $p_\perp$ in hadronic collisions in the framework of perturbative fragmentation functions, allowing an analysis at the Next to Leading Order (NLO) level which goes beyond the fixed $O(\alpha_s^3)$ perturbative theory of open charm production. We have applied HEMAS-DPM to the calculation of the prompt muon component for $E_\mu \geq 1$ TeV in air showers considering the two extreme cases of primary protons and Fe nuclei.

PACS.: 12.38.Aw; 12.38.Bx; 13.20.Fc; 13.85.Hd; 13.85.Ni; 13.85.Tp; 96.40.De; 96.40.Pq; 96.40.Tv; 96.40.Sa

Submitted to Astroparticle Physics

1 Introduction

The identification of a prompt muon component in the secondary cosmic rays coming from the decay of short–lived particles, mostly charmed particles, produced in the primary interaction is an open problem. At present, a reliable theoretical or phenomenological prediction of the prompt muon flux is still missing. Different attempts of calculation can be found in the literature [1, 2, 3, 4, 5] whose predictions vary by a few orders of magnitude one from the other, due to the different adopted models.

Here we present a new calculation of the prompt muon component in atmospheric showers, obtained by a further development of the DPMJET–II code[6], based on the Dual Parton Model, and interfaced to the shower code HEMAS[7].

Dual Parton Model (DPM) (a recent review is given in [8]) has been demonstrated to describe successfully soft hadronic processes. Various observations like rapidity plateaux, average transverse momenta rising with energy, KNO scaling violation, correlation between transverse momentum and multiplicity, and *minijet* production have pointed out that soft and hard processes are closely related. These properties are understood within the two–component Dual Parton Model [9, 10, 11]. The hard component is introduced by applying the lowest orders of perturbative hard constituent scattering[12].

The Dual Parton Model provides a framework not only for the study of hadron–hadron interactions, but also for the description of particle production in hadron–nucleus and nucleus–nucleus collisions at high energies. Within this model the high energy projectile undergoes multiple scatterings as formulated in the Glauber approach; particle production is realized by the fragmentation of colorless parton–parton chains constructed from the quark content of the interacting hadrons.

Moreover, it is straightforward to formulate the Dual Parton Model as a Monte Carlo event generator. Such a code, as for example DTUJET–93 [11] and DPMJET–II [6], is able to generate complete minimum bias events.

The applications to hadron–nucleus and nucleus–nucleus collisions, to cosmic ray hadroproduction and to cosmic ray cascade development, have been described in [6, 7]. Those papers, and the references therein, give a more detailed description of the model.

The production of charm and heavy flavour is generally calculated on the basis of perturbative QCD, for instance, in Ref.[13] . For charm production, in particular, perturbative QCD provides a rather reliable description of the photo- and electro-production of charmed hadrons. In the case of hadroproduction of charm, however, the theoretical uncertainty is larger: charmed hadrons, like other light hadrons, are mainly produced at small transverse momenta, where perturbative QCD is difficult to apply, because of the small mass of the charmed quark which does not allow such successful calculations as in the case of bottom production. In Section 3 a new approach is described in QCD, which goes beyond the strict realm of fixed order α_s^3 perturbation theory.

On the other hand, it has been demonstrated that charm production can be calculated within the framework of the Dual Parton Model (see Refs.[14, 15, 16]). In the following we will stay within this scheme. In particular we will consider one of the Monte Carlo event generator mentioned above, namely DPMJET–II. In the next Section we shall describe the charm production algorithms within the Dual Parton Model, and in Section 4 we shall compare the results of the model with the experimental data and with the QCD

calculations. The application of the model to the study of the atmospheric prompt muon component in high energy cosmic ray showers is reported in Section 5.

2 Charm production in the Dual Parton Model

In the model there are three different mechanisms where heavy flavours like charm can occur. The proper treatment of these effects is already necessary in order to get a reliable description of strange hadroproduction[17, 18] . Such mechanisms, described afterwards, are: (i) production inside the chain decay, (ii) charmed quarks produced at the ends of hard and semihard chains (minijets), and (iii) charmed quarks produced at the ends of soft sea chains. We describe these mechanisms in detail.

2.1 Charm production inside the soft chain decay

Within the Lund string fragmentation model [19] a quark–antiquark pair $q_i\bar{q}_i$, which leads to string breakup, is produced by quantum mechanical tunneling. In terms of transverse mass $m_\perp$ of the pair, the tunneling probability P is given by

$$P = \exp(-\frac{\pi m_\perp^2}{\kappa}) = \exp(-\frac{\pi m^2}{\kappa})\exp(-\frac{\pi p_\perp^2}{\kappa}) \qquad (1)$$

Starting from the suppression of strangeness production within the $q\bar{q}$ chain decay: $u\bar{u} : d\bar{d} : s\bar{s} = 1 : 1 : 0.3$ one can infer that the probability to create a $c\bar{c}$ pair is very strongly suppressed $u\bar{u} : d\bar{d} : s\bar{s} : c\bar{c} = 1 : 1 : 0.3 : 10^{-11}$, as reported in [19]. Charm production by fragmentation of chains with light flavours at their ends is therefore very unlikely to occur within the Lund model.

On the other hand, within the independent string fragmentation model BAMJET [20, 21] the probability for light or heavy flavour pair $q_i\bar{q}_i$ creation is calculated from the universal transverse energy $E_\perp$ distribution

$$P_{q\bar{q}} = C\int_{m_q}^{E_R} 2E_\perp e^{-bE_\perp} dE_\perp, \qquad E_R > m_q, \qquad (2)$$

where C is a normalization factor. The standard value for the b parameter is $b = 8$ GeV^{-1}. Using constituent quark masses we obtain the probability for a charm pair creation $P_{c\bar{c}} = \mathcal{O}(10^{-5})$

This probability is much larger than that found in JETSET [19], but even with such BAMJET fragmentation we can conclude that this contribution is not the dominant one for charm production in hadron–hadron, hadron–nucleus or nucleus–nucleus collisions.

2.2 Charm production at the ends of hard and semihard chains (minijets)

In principle, we could insert the full perturbative QCD calculation of charmed quark pairs in hard parton–parton interactions. Alternatively, we just make use of the probability

that a perturbatively produced parton pair is a $c\bar{c}$ pair. For this probability we use the expression given by Anisovich et al. [22, 23]:

$$\lambda_Q = \frac{m_q^2}{m_Q^2} \frac{1}{\ln^2(m_Q^2/\Lambda)} \tag{3}$$

where m_q and m_Q are the light and heavy constituent quark masses and Λ is the QCD scale parameter. In order to obtain the best agreement to existing data, the suppression factor λ_Q must have a value of $(5.0\ ^{+0.4}_{-0.2})\ 10^{-3}$. We then use $m_q = 0.35$ GeV/c^2, $m_Q = 1.4$ GeV/c^2 and $\Lambda = 0.2$ GeV

At hadron collision energies in the TeV range in the laboratory frame, this turns out to be the dominant mechanism of charm production in hadronic and nuclear collisions.

2.3 Charm production at the ends of soft sea chains

In the two component Dual Parton Model [11] we interpret the sea-quarks at the ends of soft sea chains as the soft non–perturbative limit of minijets. For instance, we require that the parton transverse momentum distribution of the minijets and that of the soft sea chain ends do join smoothly at the threshold transverse momentum of the minijets $p_{\perp,thr}$. Similarly, we also demand that a certain fraction of the soft sea chain ends has to carry heavy flavours.

At low energy, this probability for a $c\bar{c}$ sea quark pair should correspond to the probability for such a pair in the BAMJET chain decay. At high energy $P_{c\bar{c}}$ should instead approach the value for the semihard chains. Therefore we use:

$$P_{c\bar{c}} = C \int_{m_q}^{E_R} 2E_\perp e^{-b_c E_\perp} dE_\perp, \tag{4}$$

with

$$b_c = b + 1.3 - \log_{10}(\frac{E_{CM}}{1GeV}) \tag{5}$$

together with the condition that $p_{c\bar{c}}$ should not exceed the probability λ_c used for the semihard chains.

Actually, there are two different kinds of sea chain in the Dual Parton Model:

(i) sea-chains arising from multiple pomeron exchange in hadron–hadron collisions. The probability of having multiple pomeron exchange increases with $\sqrt{s}$, and the corresponding sea–chains are, in practice, the low $p_\perp$ limit of minijets from gluon-gluon scattering. Both processes are in fact equivalent in the topological expansion. These are the chains to which we have to apply the probability described above.

(ii) sea–chains which occur in the multiple Glauber collisions of hadrons interacting with nuclei. These chains are still obtained in single pomeron exchange also at low energy, and do not have any analogy to minijets. In this case we use, only guided by phenomenology, a $c\bar{c}$ probability *a priori* chosen to be about 10 times smaller than the one described above.

3 Charm production in perturbative QCD

The hadroproduction of heavy quarks has recently been a subject of intense studies both experimentally and theoretically, in particular as an important testing ground for QCD. A large amount of experimental data on the hadroproduction of b and c quarks and their bound states has been accumulated so far, to be compared with next-to-leading order (NLO) calculations recently available. On the theoretical side, the calculation in perturbative QCD of the differential and total cross sections to order α_s^3 has been performed[13, 24, 25, 26, 27], thus providing a firm basis for a detailed study of the properties of the bottom and charm quarks.

However, these results present a non-negligible residual renormalization/factorization scale dependence, particularly at large $p_\perp$. Furthermore, the validity of this NLO $O(\alpha_s^3)$ calculation is limited when $p_\perp \gg m$, m being the large quark mass, by the appearance of potentially large logarithms of the type $\log(p_\perp/m)$, which have to be resummed to all orders. The physical reason for that is quite clear. For example, terms of order $(\alpha_s^3)\log(p_\perp/m)$ or $(\alpha_s^4)\log(p_\perp/m)^2$ are simply related to the mass singularities originating from collinear configurations when $m \to 0$ for fixed $p_\perp$. The theoretical uncertainty associated to those corrections has been roughly estimated in [24].

A solution to this problem has recently been considered [28], following an approach based on the properties of fragmentation of a generic parton p ($p = q, g, Q$) in the heavy quark Q, after the parton has been produced inclusively in the hard collision of the two initial hadrons. The basic formula is represented by eq.7, where the partonic cross sections $\hat{\sigma}_{ij\to kX}$ at $O(\alpha_s^3)$ have been given in ref. [29], in the massless quark limit. These $\hat{\sigma}_{ij\to kX}$ introduce an explicit dependence on $p_\perp$ and on renormalization/factorization mass scales. The dependence on the heavy quark mass is then obtained through the fragmentation function of the parton $p \to Q + X$, evolved at NLO accuracy from an initial scale $\mu_0 \sim m$ (see below) to $\mu \sim p_\perp$. This approach explicitly resums potentially large terms of the kind $[\alpha_s \log(p_\perp/m)]^n$, giving a better description of the theoretical predictions at large $p_\perp$. Indeed the corresponding uncertainty is quite reduced in this region with respect to the fixed order result, due to a significantly smaller sensitivity to the relevant scales. On the other hand, because of the massless limit used for the $O(\alpha_s^3)$ kernel cross sections $\hat{\sigma}_{ij\to kX}$, this approach does not allow to recover in a simple way the limit $p_\perp \lesssim m$ of the perturbative calculation.

We will briefly review the main ideas of this analysis. According to factorization theorems the cross section for the inclusive hadroproduction of a hadron at high transverse momentum, i.e. for the process

$$H_1 + H_2 \to H_3 + X \tag{6}$$

can be written as

$$\begin{aligned} \mathrm{d}\sigma \;=\; & \sum_{i,j,k} \int \mathrm{d}x_1\, \mathrm{d}x_2\, \mathrm{d}x_3 \;\times \\ & F^i_{H_1}(x_1,\mu_F) F^j_{H_2}(x_2,\mu_F) \;\times \\ & \mathrm{d}\hat{\sigma}_{ij\to kX}(x_1,x_2,x_3,\mu_R,\mu_F) D^{H_3}_k(x_3,\mu_F) \end{aligned} \tag{7}$$

As usual, the F's are the distribution functions of the partons in the colliding hadrons, $\hat{\sigma}$ is the kernel cross section and D is the fragmentation function of the observed hadron. The

factorization mass scales μ_F of the structure and fragmentation functions are assumed to be equal for the sake of simplicity. μ_R is the renormalization scale.

Due to the presence of collinear singularities both in the initial and final state this process is not fully predictable by QCD itself. We can actually calculate the kernel cross section and the evolution of the structure and fragmentation functions, but we have to rely on some phenomenological input to obtain the latter at some given initial scale.

This situation drastically changes when we come to consider the inclusive production of a heavy quark. In this case its mass, being finite and considerably greater than Λ, makes the perturbative expansion feasible and prevents collinear singularities from appearing in the splitting vertices which involve the heavy quark. Having this in mind two approaches can be pursued in the calculation of heavy quark production.

The first one is to directly calculate in perturbation theory the process $d\hat{\sigma}_{ij\to QX}$, Q being the heavy quark and i, j the initial state *light* partons (i.e. light quarks and gluons). This kernel cross section will then be convoluted with initial state structure functions only, the final state showing no singularities of any kind. This approach has been followed in the past[13, 24, 25, 26], providing a full perturbative $O(\alpha_s^3)$ calculation. In this fixed order approach, as stated earlier, terms of the kind $\alpha_s \log(p_\perp/m)$ will appear. They are remnants of the collinear singularity screened by the finite quark mass. As quoted in ref. [24] they can grow quite large at high transverse momenta, thereby spoiling the validity of the expansion in α_s. Therefore they have to be summed to all orders.

The alternative way is to consider that when a quark, of whichever flavour, is produced at very high transverse momentum $p_\perp \gg m$ its mass plays almost no role at all in the scattering process. This is to say that mass effects in the kernel cross section are suppressed as power ratios of mass over the scale of the process. We can therefore devise a picture in which all quarks are produced in a massless fashion at the high scale $\mu_F \sim p_T \gg m$ and only successively, as their virtuality decreases, they can *fragment* into a massive heavy quark. The cross section can therefore be described by a formula analogous to eq.7, with $H_3 = Q$. The key difference to the hadroproduction case considered in eq.7 is that initial state conditions for the heavy quark fragmentation functions are now calculable from first principles in QCD at a scale of order of the heavy quark mass, and do not have to be taken from experiment.

Then using the usual Altarelli-Parisi evolution equations at NLO accuracy one finds the fragmentation functions set at any desired factorization scale μ_F. An important feature of this approach can now be appreciated. The "almost-singular" logarithmic term $\log(p_\perp/m)$ splits into two, as follows. A $\log(p_\perp/\mu_F)$ will be found in the kernel cross section $\hat{\sigma}$ which has no dependence on the heavy quark mass, according to the assumption that it is produced in a *massless* way. Moreover, by choosing $\mu_F \sim p_T$ it will not contain large logarithms and its perturbative expansion will behave correctly. The remaining part of the log will instead be lurked into the fragmentation function $D(x_3, \mu_F)$. The large $\log(\mu_F/\mu_0)$ is resummed to all orders by the evolution equations, and only the small $\log(\mu_0/m)$ provided by the initial state condition is treated at fixed order in perturbation theory. Therefore one expects a better control of the theoretical uncertainty at large $p_\perp$. On the other hand, for $p_\perp \lesssim m$ the fragmentation approach does not allow to recover easily the $O(\alpha_s^3)$ result, which, of course, holds exactly.

In this framework one can evaluate [28] the cross section for the high $p_\perp$ inclusive

hadroproduction of a bottom or charm quark. This cross section shows a reduced dependence on the renormalization/factorization scales, as a clear improvement brought by the resummation of the large logarithms of $p_\perp/m_Q$.

The above discussion refers to the production of open charm at large $p_\perp$. An independent analysis has been carried out [30] for the production of charmed mesons D and D*. Here one uses again formula 7, with H_3 = D,D*. In this case one relies on phenomenological inputs for the fragmentation functions which can be extracted from e+e- annihilation or hadron collisions at a given scale and then evoluted to NLO accuracy to the appropriate scale of $O(p_\perp)$.

In particular two completely different sets of fragmentation functions have been used to analyze the theoretical uncertainty on the input hypothesis. Indeed the resulting cross section shows very little dependence on the input model and behaves similarly to the open charm result. This is shown in fig. 1 where the D-inclusive production cross section (full line, down) is compared to the open charm inclusive cross section resulting from the fixed order $O(\alpha_s^3)$ of ref. [24] (full line, up). The two sets of dashed lines show the theoretical uncertainty from various sources (renormalization/factorization scales, sets of structure functions, initial conditions for the D fragmentation functions,...). The predicted D-inclusive distributions at large $p_\perp$ are compared in Sect. 4 with the results of the DPMJET–II generator, which are valid at smaller $p_\perp$. The two approaches are clearly mutually consistent and, combined, describe the charmed D-meson production in the full range of transverse momentum.

4 Comparison of charm production in the Dual Parton Model with experimental data and with perturbative QCD results

In the comparison of the model predictions to experiment we can use here only the data obtained in proton–proton collisions[31, 32, 33]. There are also data available from meson–proton and meson–nucleus collisions, but we have to postpone the comparison with those data, since the meson structure functions needed to calculate minijet production in meson–nucleon collisions are not yet properly included into our code DPMJET-II. Anyway, we stress that, as far as the cosmic ray showers are concerned, due to the energy dependence of the production cross section, the uncertainties associated to the meson interactions are not a significant limitation.

4.1 Comparison to data in proton–proton collisions

The total cross section for charmed meson production, as calculated from DPMJET–II, is compared in Fig.2 with the available experimental data, for collision energies $\sqrt{s}$ between 30 and 4000 GeV. These data are too poor to judge the performance of the model.

A more detailed comparison is only possible with the data of two fixed target experiments at primary proton momenta of 400 GeV/c [31] and 800 GeV/c [32].

Then, in Figs. 3 and 4 we compare the Feynman x_F and transverse momentum $p_\perp^2$ distributions obtained from the model with the data from the LEBC–EHS experiment

[31] at 400 GeV/c. We find a reasonable agreement. In order to achieve a good statistical sample, we generated 10^6 events from DPMJET–II.

In Figs. 5 and 6 we compare the Feynman x_F and transverse momentum $p_\perp^2$ distributions with the data from the LEBC–MPS experiment [32] at 800 GeV/c. Again, we find a reasonable agreement. In Table 1 we compare the production cross sections for different kinds of charmed mesons with the data from LEBC–MPS [32]. The statistical error in the calculated numbers is 5% or below, but we claim that the overall uncertainty, including systematics, is of the order of 10%. We notice that the model predictions for the relative fraction of charged and neutral D–mesons differ from the existing experimental data.

However, we can conclude that DPMJET–II has a reasonable performance as far as proton–proton collisions are concerned, in the energy region where data are available.

We turn now to hadron–nucleus and nucleus–nucleus collisions. From perturbative QCD it follows that charm production cross sections in hadron–nucleus collisions, as any other hard process, should exhibit a A^α behaviour with $\alpha = 1$, because of the fact that these processes do not see the nucleus as an opaque disk, but instead involve one individual nucleon at each interaction, (*i.e.* there is a negligible degree of shadowing). Such a behaviour has been also confirmed by some experiments [34, 35].

In Table 2 we show the charm production cross sections as calculated with DPMJET–II in p-p and p-Air collisions at different energies and we give the average transverse momenta and average Feynman x_F values of the produced charmed mesons. The error on the calculated cross sections is again of the order of 10%, while the error on the average x_F and $p_\perp$ is at the 5% level.

In Table 3 we show the charm production cross sections as calculated with DPMJET–II in p-p and p-Air collisions again. By comparing the two cross sections we find that DPMJET–II approximately reproduces the A^α behaviour with $\alpha = 1.00 \pm 0.03$ (the average air mass is $< A_{air} > \sim 14.7$).

All charmed hadrons are produced in the DPMJET–II Monte Carlo Model. In Tables 4 and 5 we give multiplicities of all charmed hadrons as produced in 10^3 p–p and p–Air collisions. For some of the charmed baryons listed here, the errors in our DPMJET–II are rather large. We observe in these Tables the ratios of neutral to charged D–mesons to be rather stable and energy independent around 2.15, the ratio between Λ_c and D^+ is again approximately energy independent around 0.5. The same energy independence seems to hold for all other possible charmed particle ratios. The energy independence of such particle ratios is also found in experiments.

4.2 Comparison with perturbative QCD calculations

In Figs. 7 to 10 we compare the inclusive $p_\perp$ cross sections of charmed mesons at different cms–energies as calculated with DPMJET–II with the results from perturbative QCD discussed in Section 3. The QCD calculations were only available at large transverse momenta ($p_\perp$ >5 GeV/c), and in a small region in Feynman x_F around $x_F = 0$. The DPMJET–II histograms were calculated in the transverse momentum region where statistically significant results could be obtained in runs with 10^6 Monte Carlo events, but only inside the x_F window considered in the QCD calculations. We find a remarkable agreement of both calculations at transverse momenta exceeding 5 GeV/c. This is a

fundamental consistency check of our results.

5 Prompt Muons from charm decay in the Cosmic Ray Cascade

We have applied the model described here to the calculation of the prompt muon component in the atmospheric showers generated by very high energy primary cosmic rays. Some characteristic features are expected for this prompt component. It differs from the ordinary muon component, generated by the decay of π and K mesons, in the fact that they come from particles with short life time, and therefore their production does not come out from the competition between interaction and decay. Thus they are expected to follow an isotropic angular distribution, as that of primary particles. For the same reason, their energy spectrum should be flatter with respect to that of ordinary muons, having a spectral index differing by one unit. It is well known that an additional $1/E$ factor is coming from the decay probability of longer life mesons: due the relativistic expansion of time, the higher is the meson energy, the larger is the chance to undergo an inelastic interaction. Prompt muons are also expected to be produced at a higher average transverse momentum than ordinary muons. The detection of a prompt component in passive experiments, such as the large detectors underground, still remains an important measurement to achieve an experimental insight of the heavy flavour production in the forward region at very high energy. The existing results are not conclusive (see for instance ref. [1, 36, 37]).

In order to perform this study, we made use of the HEMAS shower code interfaced to DPMJET-II, as described in [7]. We have generated showers from two extreme primary mass components, protons and iron nuclei, in the energy range 20–10^5 TeV/particle according to a typical primary energy spectrum falling as $E^{-2.7}$ up to about 2000 TeV (the "knee" region), and as $E^{-3.0}$ above the knee. The lower energy limit comes from practical considerations, since the probability of generating prompt muons at lower energy turns out to be very small. We have generated an equivalent number of showers equal to $3 \cdot 10^5$ for each mass component, using a HP-UX9000 platform. These primaries are assumed to be isotropically distributed in solid angle. However we have limited our simulation in the zenithal range $0 \div 60°$, since the present version of HEMAS does not take into account the earth curvature. We have recorded all muons of energy $E_\mu \geq 1$ TeV produced in the atmospheric showers together with all informations concerning the kinematics of their parents, up to the first inelastic interactions. In our simulation, the shower is sampled in atmosphere at the vertical height of 2000 m above the sea level. In the following, we will present the main results concerning the differences between ordinary muons and prompt muons.

In Figs. 11 and 12 we show the calculated average muon yield ($E_\mu \geq 1$ TeV) for the prompt and non–prompt component, as a function of the total energy of primary protons. We show the results both for the atmospheric muons and for those of them which survive at an average depth in standard rock of 3800 $hg\ cm^2$ (such as the case of the underground laboratory of Gran Sasso, for example). We remind here that the HEMAS–DPMJET code is interfaced to the muon propagation code in standard rock described in ref. [38].

Since the non–prompt component has a $sec(\theta)$ angular dependence in the considered solid angle, the yield for this component has been referred to the vertical. We notice that almost at all energies the prompt/non–prompt ratio remains of the order of $10^{-4} \div 10^{-3}$. Furthermore, we also notice that the relative fraction of survived muons is higher for the prompt component, as expected in the case of a flatter energy spectrum. This will be shown in more detail later.

Similar plots for the case of primary Fe nuclei are shown in Figs. 13 and 14. Here we show the average yield per nucleon, as a function of energy/nucleon, in order to point out the substantial validity of the surperposition model, according to which a nucleus of mass number A and total energy E behaves like A nucleons of energy E/A. This scheme is well verified in the case of the prompt muon component, and it is quite reasonable, due to the negligible degree of shadowing as already remarked in Section 4.2. The same observations expressed in the case of primary protons concerning the muon energy spectrum and survival probability hold here.

As a confirmation of our guesses about the muon energy spectrum, in Fig. 15 we show the calculated energy distribution for non–prompt and prompt muons in atmosphere from primary protons. The continuous lines are simple power laws $E^{-\gamma}$ with γ=3.7 for the non–prompt component, and γ=2.7 for the prompt one, marked just as a guide for the eye (a spectral index slowly changing with the energy would give a more reasonable fit). The simulated statistics does not allow to extrapolate reliably at muon energies above a few hundreds of TeV, but at this stage it is reasonable to assume that this behaviour continues up to thousands of TeV, where the prompt component will eventually overcome the non–prompt one. Similar results are obtained for primary Fe nuclei, as shown in Fig. 16.

The difference in the angular distribution between the prompt and non–prompt muon components is evident from Figs. 17 and 18, where the prompt/non–prompt ratio in atmosphere is plotted as a function of the cosine of the zenith angle in the case of primary protons and primary Fe nuclei respectively. The $sec(\theta)$ dependence of the ordinary muons and the flat distribution of prompt muons are well reproduced by the model.

It is also interesting to examine the prompt/non–prompt ratio for underground muons. In Figs. 19 and 20 we plot this ratio as a function of the cosine of the zenith angle for different depths. These have been obtained using the survival probabilities in standard rock from ref.[38]. Due to the different steepness of the energy spectra of prompt and non–prompt muons, the very large depth are favoured for the search for prompt muons. In our plots angle and depth are uncorrelated, but in real cases there is an obvious correlation between depth and $sec(\theta)$, and therefore the search at large zenith angles is highly convenient (see ref. [37]). According to our calculations, it seems that only above 7000 hg/cm^2 there is some possibility to identify a prompt (*i.e.* isotropic) muon component underground, provided that all systematics is kept below the 1% level. We expect that also the residual energy of underground muons should reflect the different nature of prompt muons, however, the simulated statistics does not allow us to reach any conclusion on this point.

Finally, in Figs. 21 and 22 we show the muon lateral displacement (i.e. the distribution of the distance R_μ from the shower axis) in atmosphere for primary protons and Fe nuclei respectively. Apart from the fact that the percentage of the prompt muons is quite small,

we notice that their lateral distribution is even narrower than that of the ordinary muons. This apparently contradicts the naive expectation that prompt muons should exhibit a larger $< R_\mu >$ than ordinary muons because of the the fact that the D mesons are produced with an average $p_\perp$ larger than that of pions and kaons. This is true, but we have to remind that the muon lateral displacement depends mostly on two factors: the muon angle with respect to the shower axis (approximately given by $p_\perp/E_\mu$) and the slant distance travelled by the muon from the production point down to the atmospheric sampling level. For prompt muons we have, with respect to the non–prompt ones: larger $p_\perp$, much larger energy (thus a smaller angle $p_\perp/E_\mu$) but also a slightly larger production height H, since we find that they are preferentially produced in the first stages of the shower development (at later stages the energy is degraded and the production cross section is rapidly decreasing). If we describe the shower evolution in terms of Generations (*e.g.* primary has generation number G=0, the products of the first interaction have G=1, those of the second interaction have G=2, etc.), then we obtain, for example, that in the energy range $2\cdot 10^3 \div 2\cdot 10^4$ TeV, non–prompt muons from primary protons have $< G > = 4.9$ while prompt muons have $< G > \doteq 4.2$, corresponding to a larger production height. However, the combined effects of different H, $p_\perp$ and E_μ result in a lateral distribution for prompt muons which do not overcome that of ordinary muons at large distances. In Tables 6 and 7 we summarise the average E_μ, $p_\perp$ and R_μ as obtained from our model.

6 Conclusions

We succeeded in including a charm production mechanism in a Monte Carlo model, based on the two component Dual Parton Model, for cosmic rays interaction in the atmosphere. The parameters of the model have been chosen in such a way to give the most probable values for the cross section, as allowed by the (poor) existing data from accelerator experiments. The agreement at high $p_\perp$ with QCD calculations is the only possible cross check to give us some confidence on the reliability of the model, within the considered hypotheses. As shown in this paper, this has been successfully achieved in our work. In this respect the models proposed in 1983 in ref. [1] seem too optimistic, in the light of present knowledge, in the estimate of both the production cross section and the charmed baryon/Λ ratio.

The results obtained with our model confirm most of the expectations concerning the general features of the prompt muon component in the secondary cosmic rays coming from charmed particle decay. However, we have to recognize that the quantitative predictions are such to consider as extremely difficult the identification of a prompt component by existing underground experiments even with large statistics, due to the high control of systematics requested in any detailed analysis concerning the angular distribution, unless unexpected and exotic mechanisms enhancing charm production (not considered here) occur. Another possibility, not discussed in this work, is the analysis of the double muon events, which correspond to a higher primary energy, and this is a way to enhance the prompt/non–prompt ratio. Both this possibility and the search for new phenomena are, in our opinion, good reasons to encourage and continue the search for prompt muons in cosmic ray experiments.

References

[1] J.W. Elbert, T.K. Gaisser and T. Stanev, *Phys. Rev.* D27(1983)1448.

[2] C. Castagnoli et al.,, *Il Nuovo Cimento* A82,(1984)78.

[3] L.V. Volkova et al.,, *Il Nuovo Cimento* 10C,(1987)465.

[4] E. Zas et al.,, *Astroparticle Phys.* 1,(1993)297.

[5] M. Thunman, G. Ingelman and P. Gondolo, Uppsala University Preprint TSL/ISV-95-0112, to appear in the proceedings of "Trends in Astroparticle Physics", Stockholm, 1994 1995.

[6] J. Ranft, *Phys. Rev.* D 51(1995)64.

[7] G.Battistoni, C.Forti and J.Ranft, *Astroparticle Phys.* 3(1995)157.

[8] A. Capella, U. Sukhatme,Chung I Tan and J. Tran Thanh Van, *Phys. Repts.* 236(1994)225.

[9] A. Capella, J. Tran Thanh Van and J. Kwiecinski, *Phys. Rev. Lett.* 58(1987)2015.

[10] P. Aurenche, F. W. Bopp, A. Capella, J. Kwiecinski, M. Maire, J. Ranft and J. Tran Thanh Van, *Phys. Rev.* D45(1992)92.

[11] F. W. Bopp, D. Pertermann, R. Engel and J. Ranft,, *Phys. Rev.* D 49(1994)3236.

[12] B. L. Combridge, J. Kripfganz and J. Ranft, *Phys. Lett.* 70B(1977)234.

[13] P. Nason, S. Dawson and R. K. Ellis, *Nucl. Phys. B* B 303(1988)607.

[14] Yu.M. Shabelski, *Z. Phys.* C 57(1993)409.

[15] A.B.Kaidalov and O.I.Piskunova , *Sov.J.Nucl.Phys.* 43(1986)994.

[16] A. De Rujula, E. Fernandez and J.J.Gomez–Cadenas , CERN preprint CERN–TH 6452 1992.

[17] J. Ranft, A. Capella and J. Tran Thanh Van, *Phys. Lett.* B320(1994)346.

[18] A. Capella and J. Tran Thanh Van and J. Ranft, *Nucl. Phys. B* A 566(1994)511c.

[19] T. Sjöstrand, CERN Report CERN–TH.6488/92, 1992.

[20] S. Ritter, *Comput. Phys. Commun.* 31(1984)393.

[21] J. Ranft and S. Ritter, *Acta Phys. Pol. B* 11(1980)259.

[22] V.V. Anisovich, M.G.Huber, M.N.Kobrinsky and B.Ch. Metsch , *Phys. Rev.* D 42(1990)3045.

[23] V.V. Anisovich and B.Ch. Metsch , *Phys. Rev.* D 46(1992)3195.

[24] P. Nason, S. Dawson and R. K. Ellis, *Nucl. Phys. B* B 327(1989)49.

[25] W. Beenakker, H. Kuijf, W.L. van Neerven and J. Smith, *Phys. Rev.* D 40(1989)54.

[26] W. Beenakker, W.L. van Neerven, R. Meng, G.A. Schuler and J. Smith, *Nucl. Phys. B* B 351(1991)507.

[27] M.L. Mangano, P. Nason and G. Ridolfi, *Nucl. Phys. B* B 373(1992)295.

[28] M. Cacciari and M. Greco, *Nucl. Phys. B* B 421(1994)530.

[29] F. Aversa, P. Chiappetta, M. Greco and J.Ph. Guillet, *Nucl. Phys. B* B 327(1989)105.

[30] M. Cacciari, M. Greco and A. Tanzini, *In preparation* (1995).

[31] M. Aguilar–Benitez et al. LEBC–EHS Collaboration, *Z. Phys.* C 40(1988)321.

[32] R. Ammar et al. LEBC–MPS Collaboration, *Phys. Rev. Lett.* 61(1988)2185.

[33] O. Botner et al. , *Phys. Lett.* B 236(1990)488.

[34] G.A. Alves et al. , *Phys. Rev. Lett.* 70(1993)722.

[35] M. Adamovich et al., WA82 Collaboration , *Phys. Lett.* B 284(1992)453.

[36] Yu.M. Andreyev, V.I. Gurentsov, and I.M. Kogai, *Proceedings of the 20st ICRC, Moscow* 6(1987)200.

[37] A. Castellina, B. D'Ettorre Piazzoli, G. Mannocchi, P. Picchi and S. Vernetto, *Il Nuovo Cimento* 8C, N.1(1985)93.

[38] P.Lipari and T.Stanev, *Phys. Rev.* D44(1991)3543.

Table 1. Comparison of charm production in proton–proton collisions at 800 GeV/c as measured by the LEBC–MPS Collaboration [32] with the results of DPMJET–II. We report in the first column the average multiplicity $< n >$, and in the second one the cross section. The experimental average charged multiplicity in minimum bias events is 10.26 $\pm$0.15 to be compared with the DPMJET–II results (including single diffractive interactions) which give 9.56 $\pm$ 0.05. The error on the calculated cross sections is of the order of 10% (see text).

	DPMJET–II	DPMJET–II	Exp.[32]
Particle	$< n >$	σ [μb]	σ [μb]
D^0	$3.86 \cdot 10^{-4}$	13.1	
D^+	$1.54 \cdot 10^{-4}$	5.4	
D^-	$1.86 \cdot 10^{-4}$	6.3	
$\bar{D}^0$	$3.68 \cdot 10^{-4}$	12.5	
D_c^+	$0.90 \cdot 10^{-4}$	3.1	
D_c^-	$0.88 \cdot 10^{-4}$	3.1	
$D\bar{D}$	$6.30 \cdot 10^{-4}$	21.4	$24\ ^{+5}_{-4}$
$D/\bar{D}$	$12.72 \cdot 10^{-4}$	43.2	$48\ ^{+10}_{-8}$
$D^+/\bar{D}^-$	$3.40 \cdot 10^{-4}$	17.6	26 ± 4
$D^0/\bar{D}^0$	$7.54 \cdot 10^{-4}$	25.6	$22\ ^{+9}_{-7}$

Table 2. Charm production in proton–proton and proton–Air collisions as calculated with DPMJET–II. The error on the calculated cross sections is of the order of 10%, while that on the average $p_\perp$ and x_F is at 5% level (see text).

	p	$\sqrt{s}$	$\sigma_{D\bar{D}}$	$< x_F^{D/\bar{D}} >$	$< p_\perp >^{D/\bar{D}}$
Collision	[TeV/c]	[GeV]	[μb]		[GeV/c]
p–p	0.4	27.4	7.6	0.14	0.87
p–p	0.8	38.8	21.4	0.13	0.89
p–p	10.	137	131	0.104	1.04
p–p	100.	433	394	0.088	1.22
p–p	1000.	1370	1026	0.07	1.42
p–Air	0.4	27.4	103	0.12	0.84
p–Air	0.8	38.8	337	0.13	1.09
p–Air	10.	137	1686	0.099	1.07
p–Air	100.	433	6296	0.060	1.34
p–Air	1000.	1370	15207	0.057	1.52

Table 3. Charm production in proton–proton and proton–Air collisions as calculated with DPMJET–II. In the last column it is given the ratio of the charm production cross section in proton–Air to that in proton–proton collisions. We find approximately an A^{α} behaviour with $\alpha = 1$. The statistical error on multiplicities is of the order of 5%, and the uncertainty on the cross sections is of 10%.

p	σ_{inel}^{pp}	$n_{D\bar{D}}^{pp}$	$\sigma_{D\bar{D}}^{pp}$	$\sigma_{D\bar{D}}^{p-Air}$	Ratio
[TeV/c]	[mb]		[μb]	[μb]	
0.4	33	$2.3 \cdot 10^{-4}$	7.59	102.1	13.6
0.8	34	$6.3 \cdot 10^{-4}$	21.4	337	15.7
10	39	$3.36 \cdot 10^{-3}$	131	1686	12.9
100	45	$8.75 \cdot 10^{-3}$	394	6296	16.0
1000	54	$1.90 \cdot 10^{-2}$	1026	15207	14.8
10000	69	$3.60 \cdot 10^{-2}$	2484	36572	14.7

Table 4. Production of all kinds of charmed hadrons in proton–proton collisions as calculated with DPMJET–II at different energies. We give the average multiplicities calculated in 10^3 p–p collisions.

	1 TeV	10 TeV	100 TeV	1000 TeV
D^0	0.73	2.8	6.2	13.4
D^+	0.24	1.3	2.9	6.2
D^-	0.25	1.4	3.3	6.3
$\bar{D}^0$	0.68	2.7	6.0	13.7
D_s^+	0.09	0.51	1.3	2.4
D_s^-	0.13	0.47	1.1	2.4
Λ_c^+	0.11	0.57	1.42	2.9
Ξ_c^+	0.00	0.04	0.31	0.54
Ξ_c^0	0.03	0.08	0.16	0.44
Σ_c^{++}	0.00	0.10	0.18	0.48
Σ_c^+	0.01	0.07	0.17	0.45
Σ_c^0	0.01	0.07	0.31	0.42
$\bar{\Lambda}_c^-$	0.07	0.44	1.31	2.4
$\bar{\Xi}_c^-$	0.01	0.10	0.19	0.46
$\bar{\Xi}_c^0$	0.01	0.11	0.26	0.47
$\bar{\Sigma}_c^{--}$	0.02	0.07	0.20	0.42
$\bar{\Sigma}_c^-$	0.03	0.08	0.29	0.41
$\bar{\Sigma}_c^0$	0.03	0.12	0.18	0.44
D^0/D^+	3.04	2.17	2.14	2.16
Λ_c^+/D^+	0.46	0.44	0.49	0.48

Table 5. Production of all kinds of charmed hadrons in proton–Air collisions as calculated with DPMJET–II. at different energies. We give the average multiplicities calculated in 10^3 p–Air collisions.

	1 TeV	10 TeV	100 TeV	1000 TeV
D^0	0.98	4.4	13.4	24.9
D^+	0.54	2.1	4.5	13.4
D^-	0.64	2.3	5.5	11.9
$\bar{D}^0$	0.98	4.5	12.6	24.9
D_s^+	0.23	0.90	1.6	4.3
D_s^-	0.16	0.70	1.1	4.5
Λ_c^+	0.34	1.0	2.5	6.6
Ξ_c^+	0.03	0.1	0.4	0.9
Ξ_c^0	0.05	0.1	0.5	0.7
Σ_c^{++}	0.05	0.2	0.4	0.9
Σ_c^+	0.03	0.1	0.4	0.7
Σ_c^0	0.04	0.2	0.3	0.4
$\bar{\Lambda}_c^-$	0.33	1.3	1.6	5.9
$\bar{\Xi}_c^-$	0.03	0.1	0.4	0.9
$\bar{\Xi}_c^0$	0.06	0.00	0.1	0.6
$\bar{\Sigma}_c^{--}$	0.05	0.00	0.6	1.2
$\bar{\Sigma}_c^-$	0.06	0.1	0.2	0.5
$\bar{\Sigma}_c^0$	0.03	0.1	0.8	0.6
D^0/D^+	1.65	2.09	2.98	2.20
Λ_c^+/D^+	0.63	0.48	0.56	0.48

Table 6. Average values of energy, E_μ, transverse momentum, $p_\perp$, and distance from shower axis, R_μ, for atmospheric muons ($E_\mu \geq 1$ TeV) produced by proton primaries in the range 20-10^5 TeV.

	E_μ (TeV)	$p_\perp$ (GeV/c)	R_μ (m)
prompt muons	4.0 ± 0.2	0.59 ± 0.01	7.8 ± 0.2
non–prompt muons	1.931 ± 0.001	0.536 ± 0.001	10.66 ± 0.01

Table 7. Average values of energy, E_μ, transverse momentum, $p_\perp$, and distance from shower axis, R_μ, for atmospheric muons ($E_\mu \geq 1$ TeV) produced by primary Fe nuclei in the range 20-10^5 TeV/nucleus.

	E_μ (TeV)	$p_\perp$ (GeV/c)	R_μ (m)
prompt muons	2.6 ± 0.1	0.67 ± 0.02	9.8 ± 0.4
non–prompt muons	1.814 ± 0.001	0.549 ± 0.001	11.76 ± 0.01

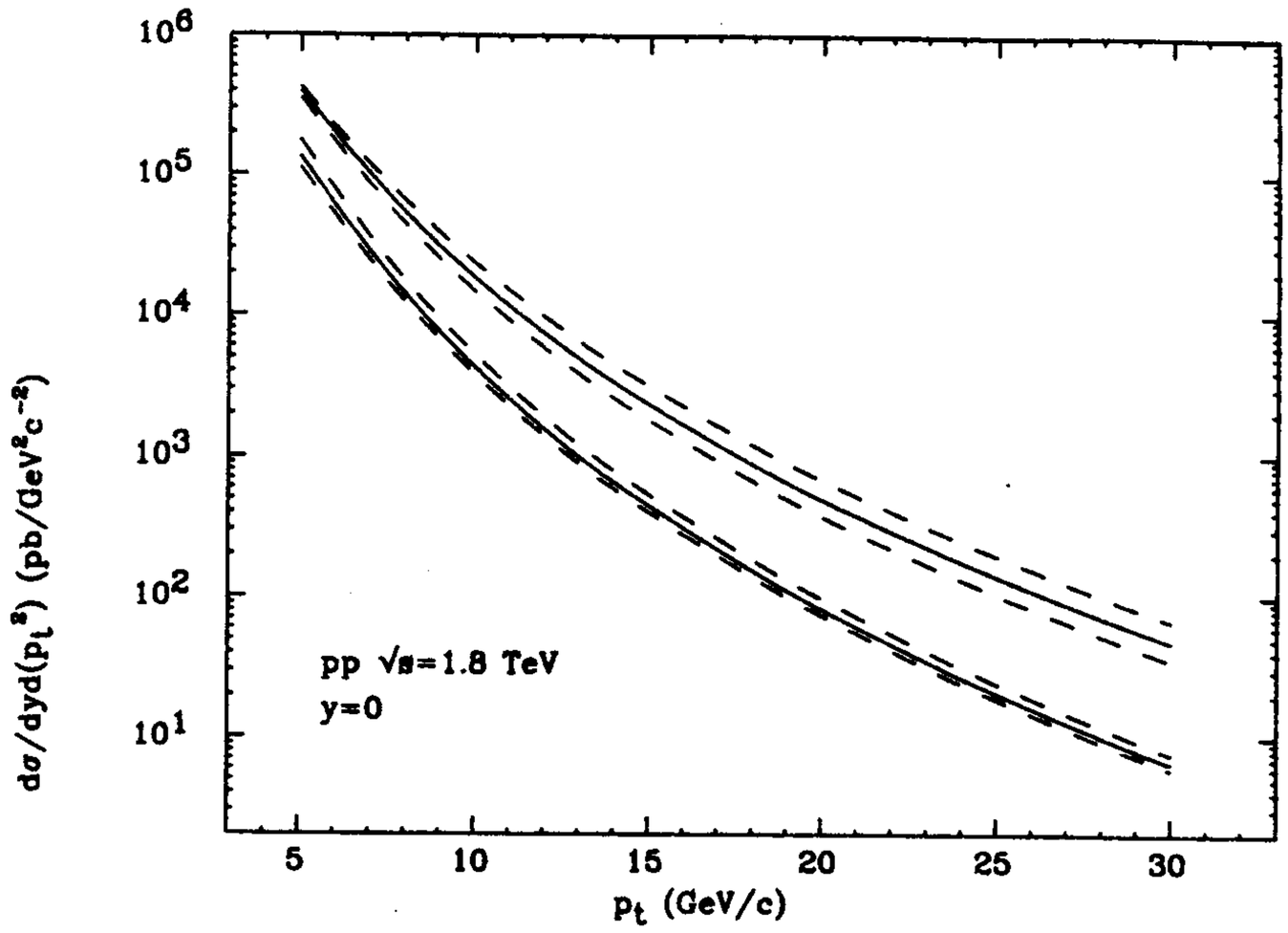

Figure 1: The D-inclusive production cross section (full line, down) is compared to the open charm inclusive cross section resulting from the fixed order $O(\alpha_s^3)$ (full line, up). The two sets of dashed lines show the theoretical uncertainty from various sources (renormalization/factorization scales, sets of structure functions, initial conditions for the D fragmentation functions,etc., as described in the text.).

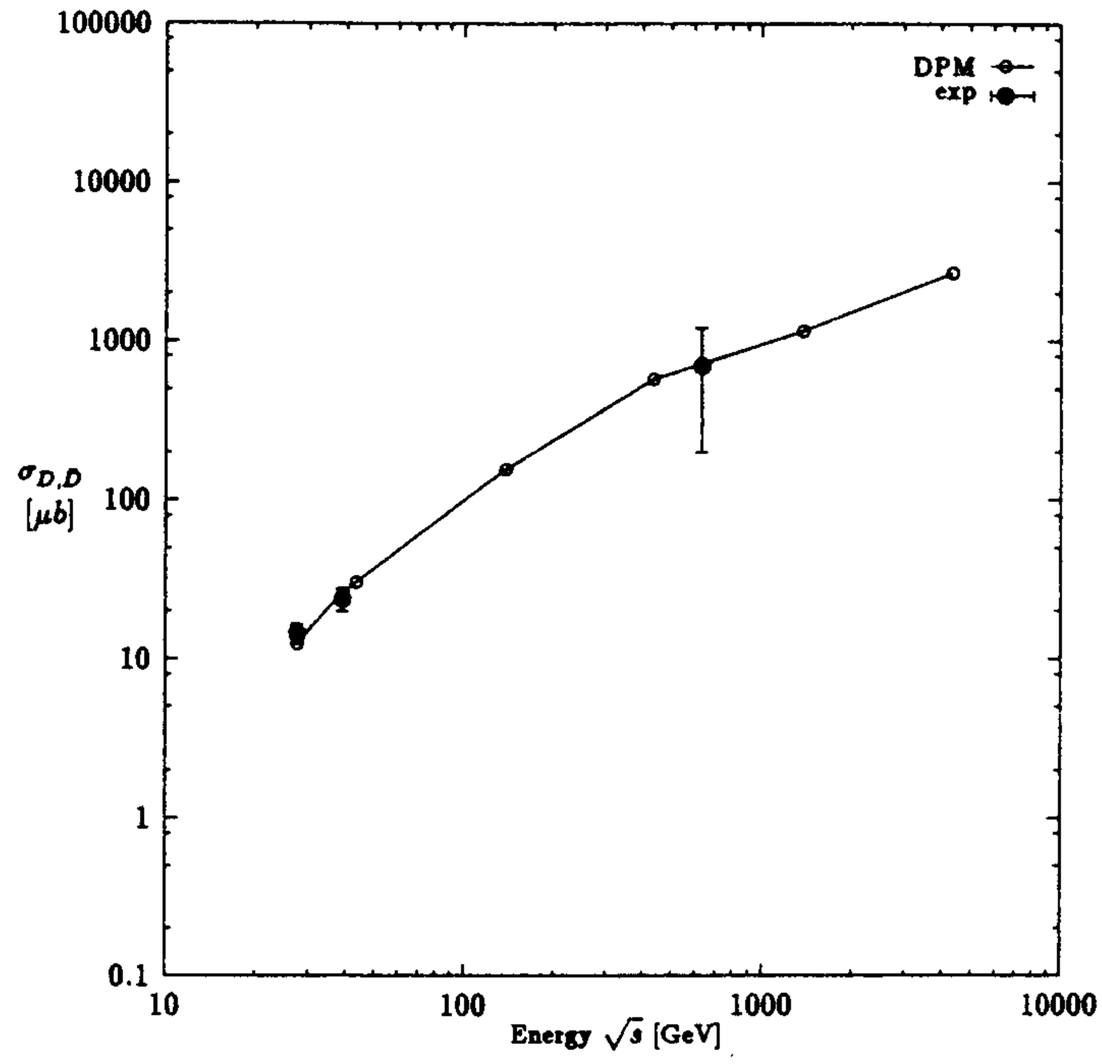

Figure 2: Total charm production cross sections in proton–proton collisions. The cross sections calculated with the Dual Parton Model code DPMJET–II are compared to experimental data[31, 32, 33]. A line is drawn to guide the eye.

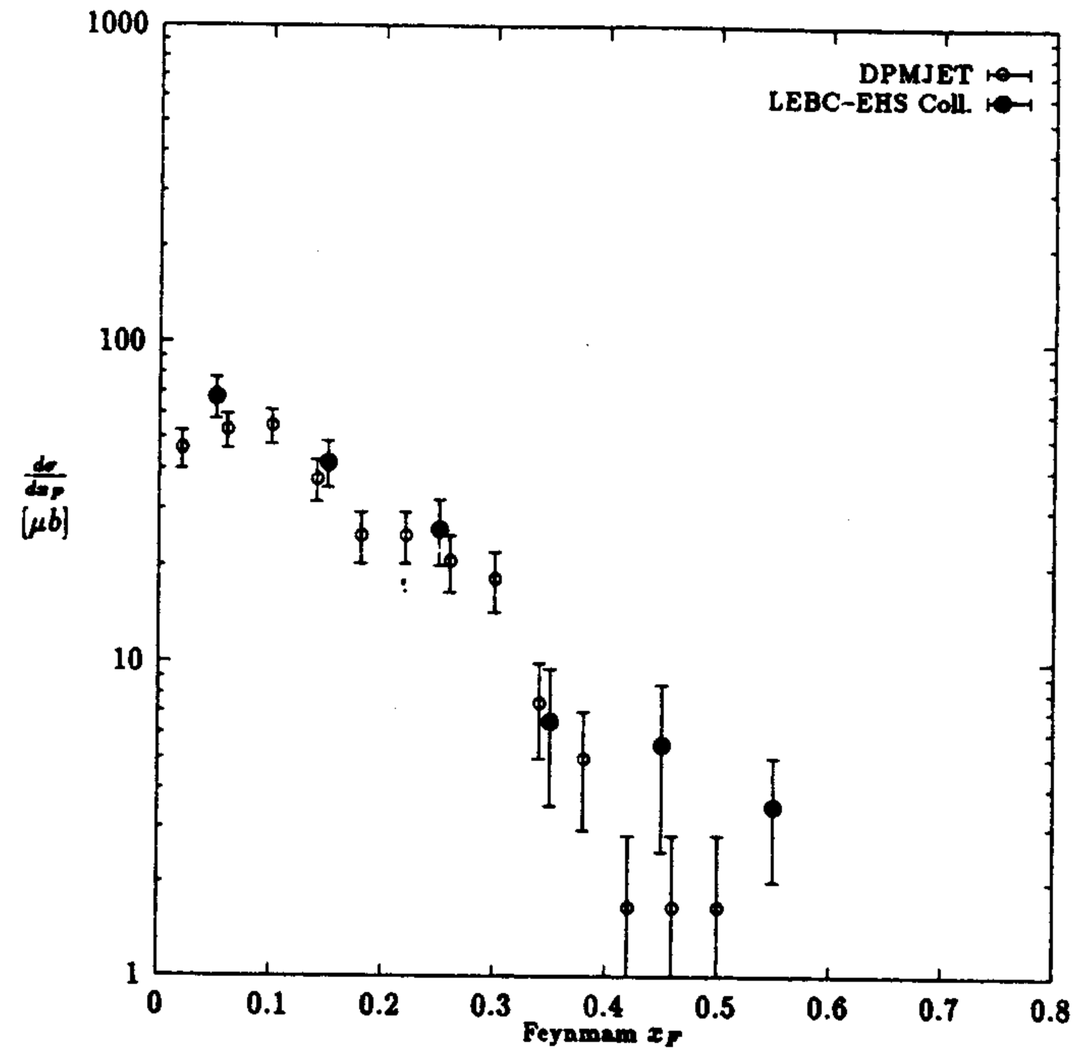

Figure 3: The inclusive cross section for the production of charmed mesons as a function of Feynman–x_F. We compare the DPMJET–II calculation with data from the LEBS–EHS Collaboration [31] at 400 GeV.

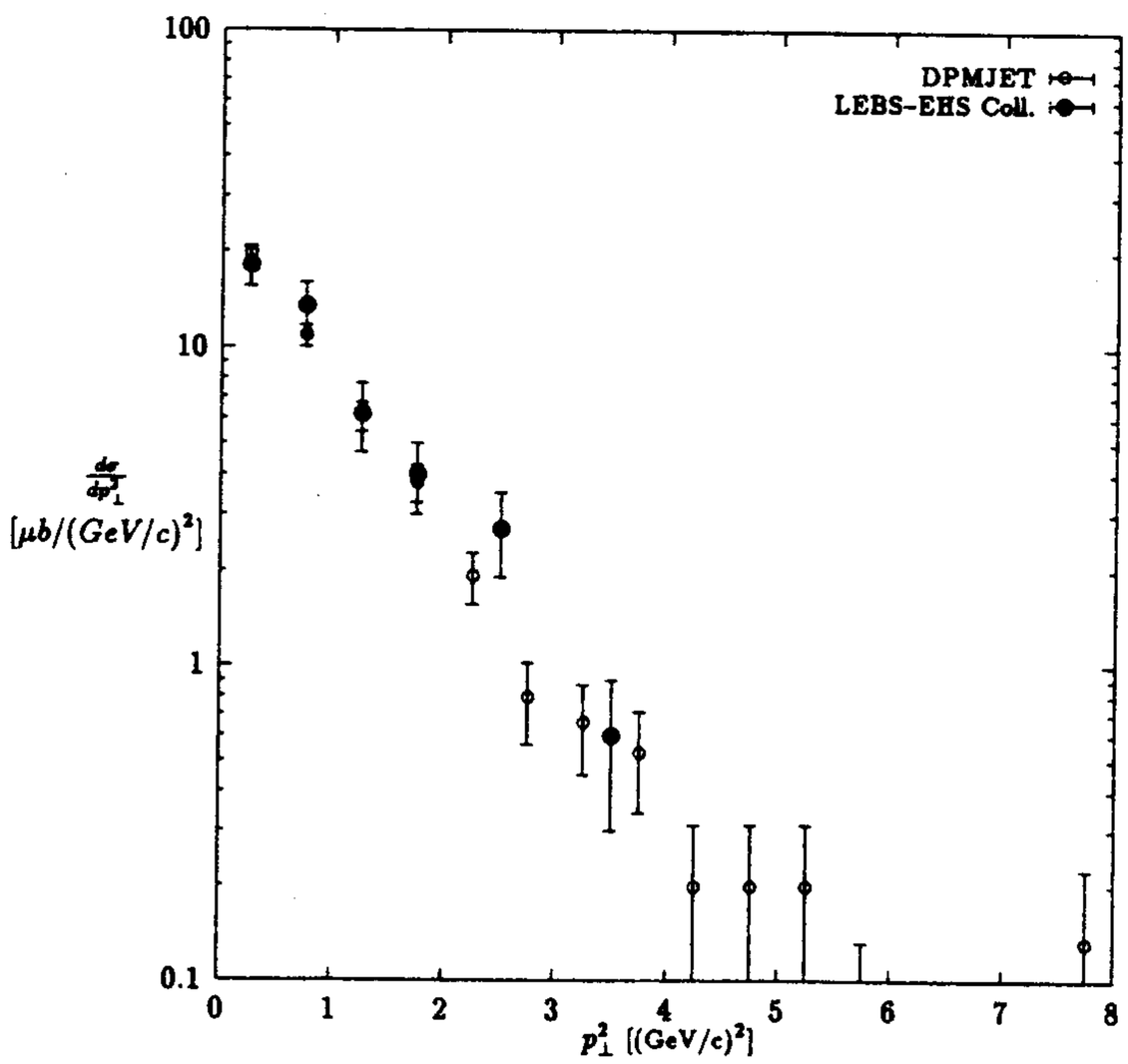

Figure 4: The inclusive cross section for the production of charmed mesons as a function of $p_\perp^2$. We compare the DPMJET–II calculation with data from the LEBS–EHS Collaboration [31] at 400 GeV.

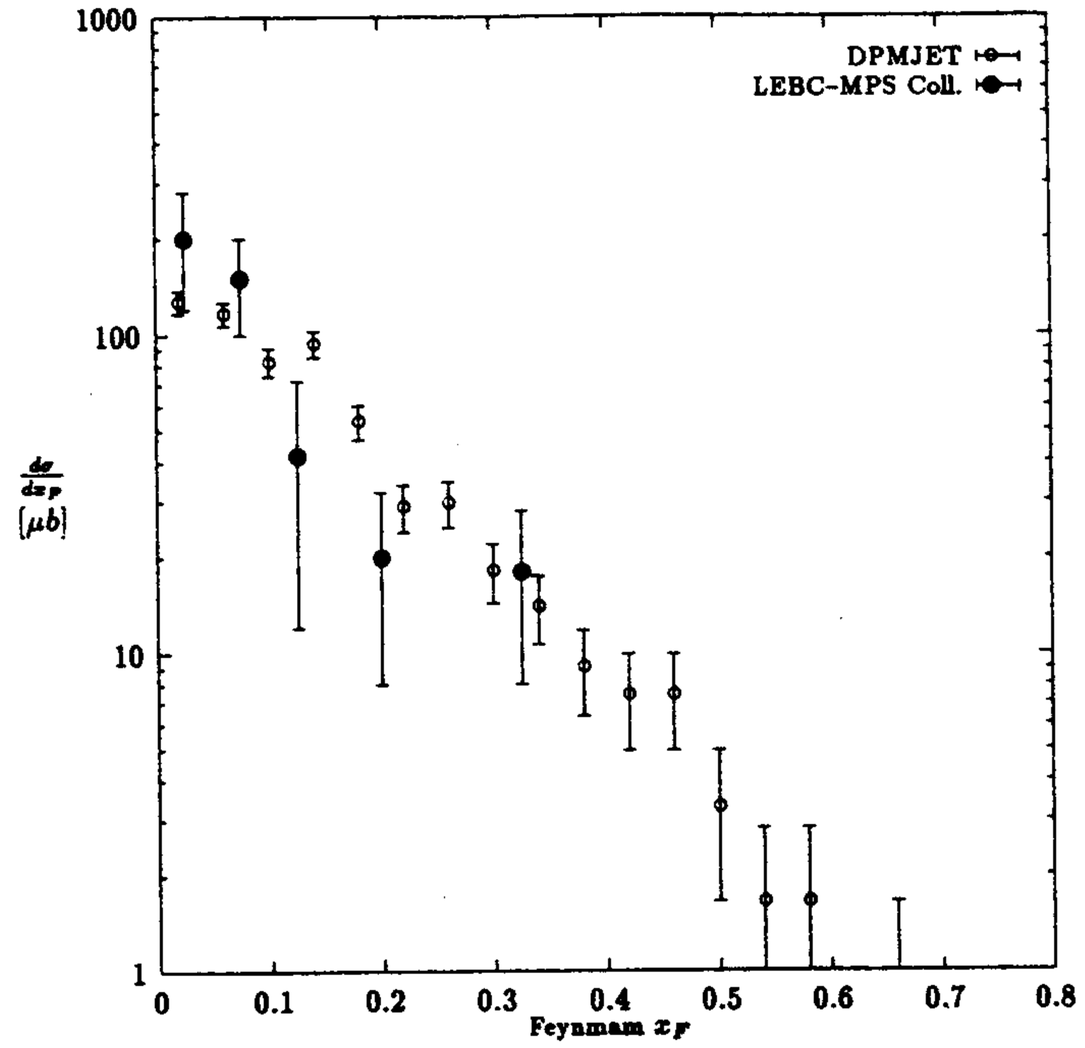

Figure 5: The inclusive cross section for the production of charmed mesons as a function of Feynman–x_F. We compare the DPMJET–II calculation with data from the LEBS–MPS Collaboration [32] at 800 GeV.

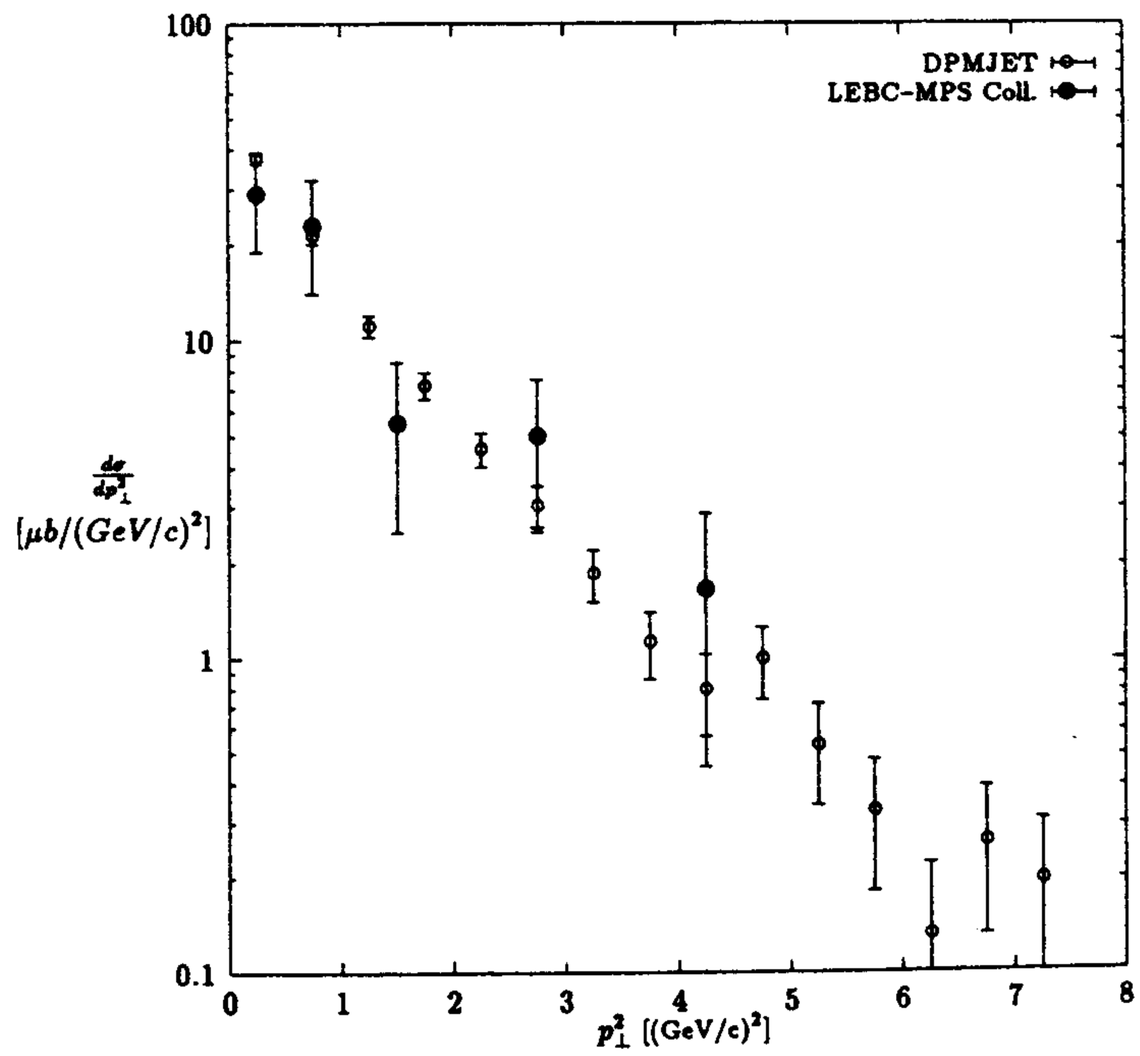

Figure 6: The inclusive cross section for the production of charmed mesons as a function of $p_\perp^2$. We compare the DPMJET–II calculation with data from the LEBS–MPS Collaboration [32] at 800 GeV.

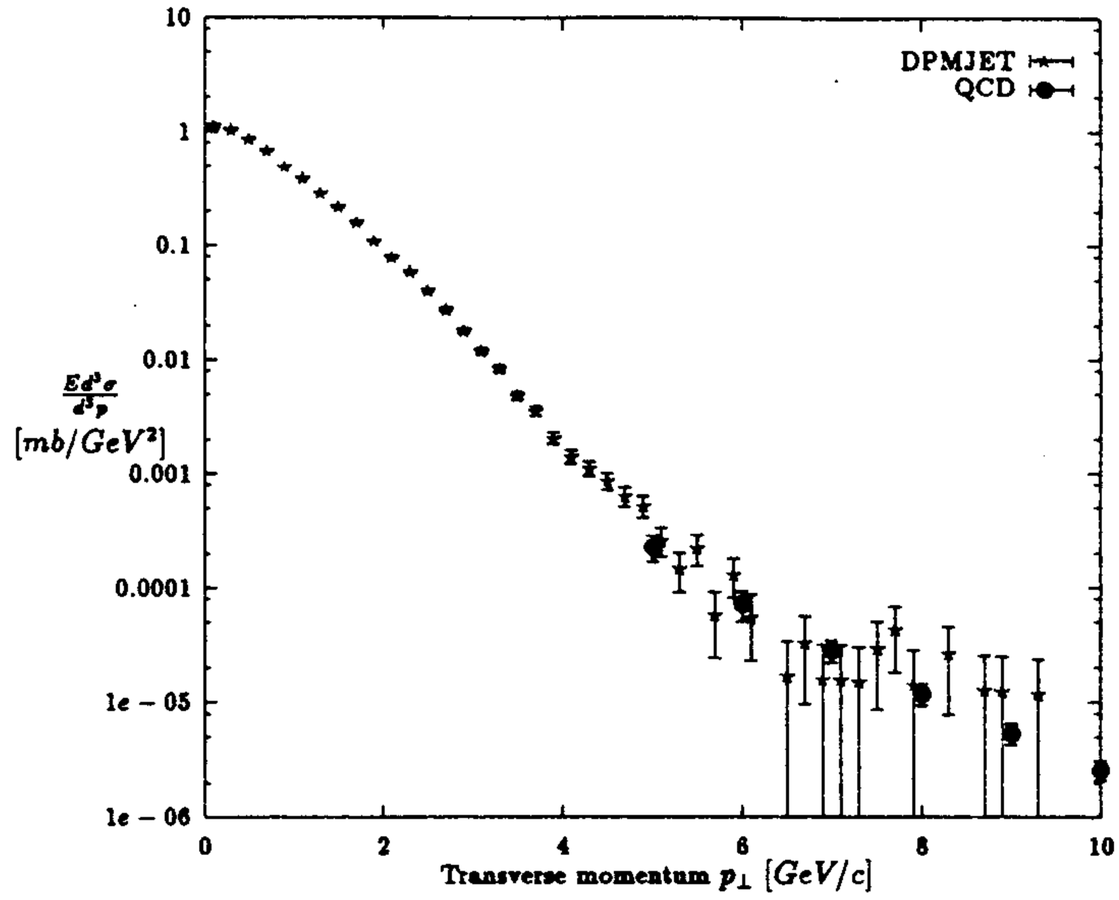

Figure 7: The inclusive cross section for the production of charmed mesons in proton–proton collisions, at 500 GeV c.m. energy, as a function of the transverse momentum $p_\perp$. The calculation using the DPMJET–II code is compared at transverse momenta above 5 GeV/c with perturbative QCD calculations. In both calculations the $p_\perp$ cross section is the result of an integration over Feynman x_F in the range -0.45 $< x_F <$ 0.45.

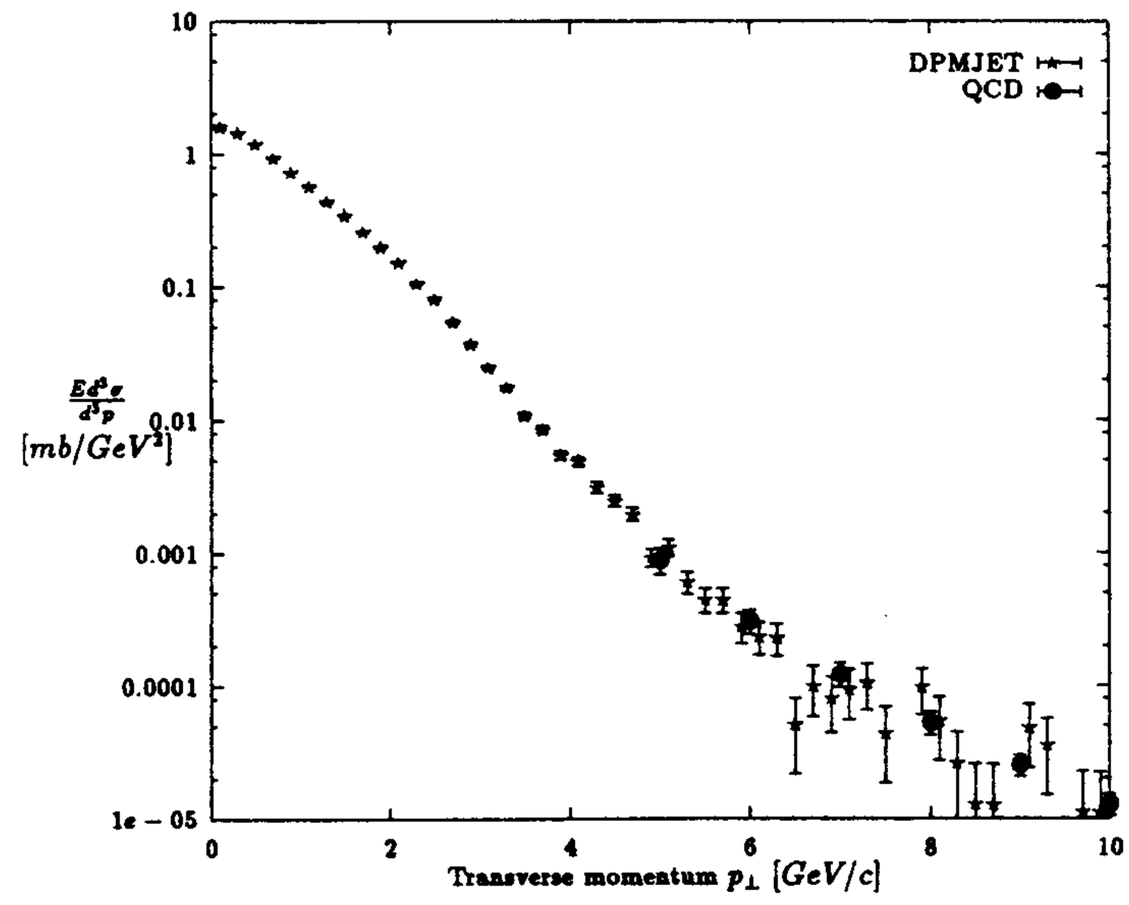

Figure 8: The inclusive cross section for the production of charmed mesons in proton–proton collisions, at 1 TeV c.m. energy, as a function of the transverse momentum $p_\perp$. The calculation using the DPMJET–II code is compared at transverse momenta above 5 GeV/c with perturbative QCD calculations. In both calculations the $p_\perp$ cross section is the result of an integration over Feynman x_F in the range -0.45 $< x_F <$ 0.45.

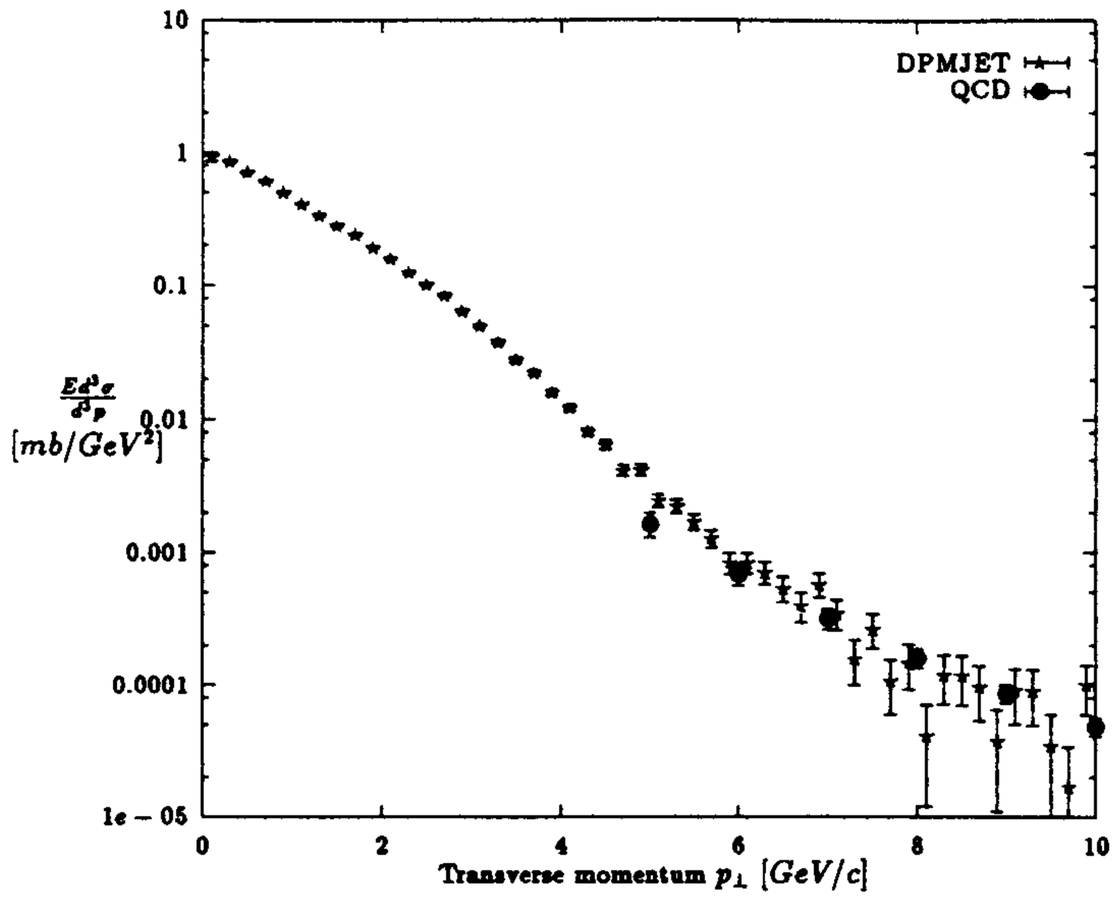

Figure 9: The inclusive cross section for the production of charmed mesons in proton–proton collisions, at 5 TeV c.m. energy, as a function of the transverse momentum $p_\perp$. The calculation using the DPMJET–II code is compared at transverse momenta above 5 GeV/c with perturbative QCD calculations. In both calculations the $p_\perp$ cross section is the result of an integration over Feynman x_F in the range -0.0108 $< x_F <$ 0.0108.

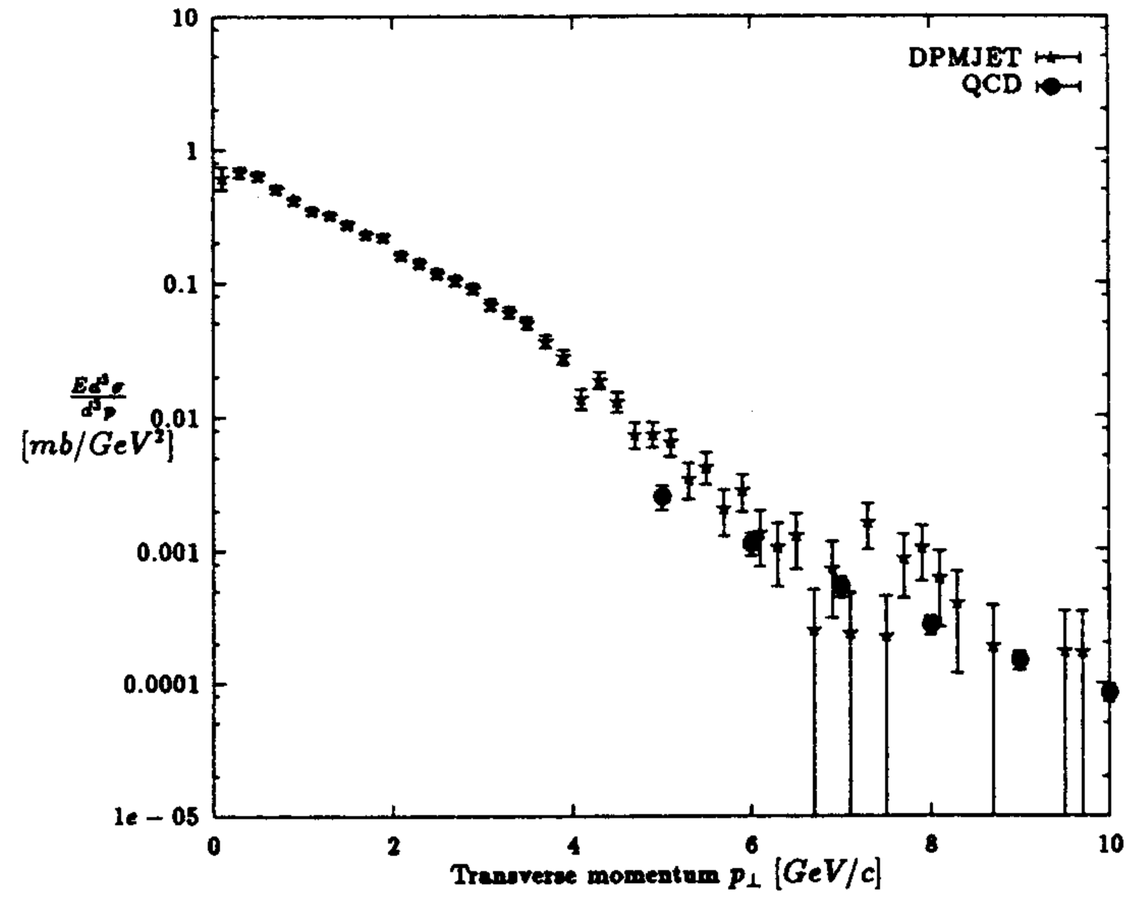

Figure 10: The inclusive cross section for the production of charmed mesons in proton–proton collisions, at 10 TeV c.m. energy, as a function of the transverse momentum $p_\perp$. The calculation using the DPMJET–II code is compared at transverse momenta above 5 GeV/c with perturbative QCD calculations. In both calculations the $p_\perp$ cross section is the result of an integration over Feynman x_F in the range -0.0045 $< x_F <$ 0.0045.

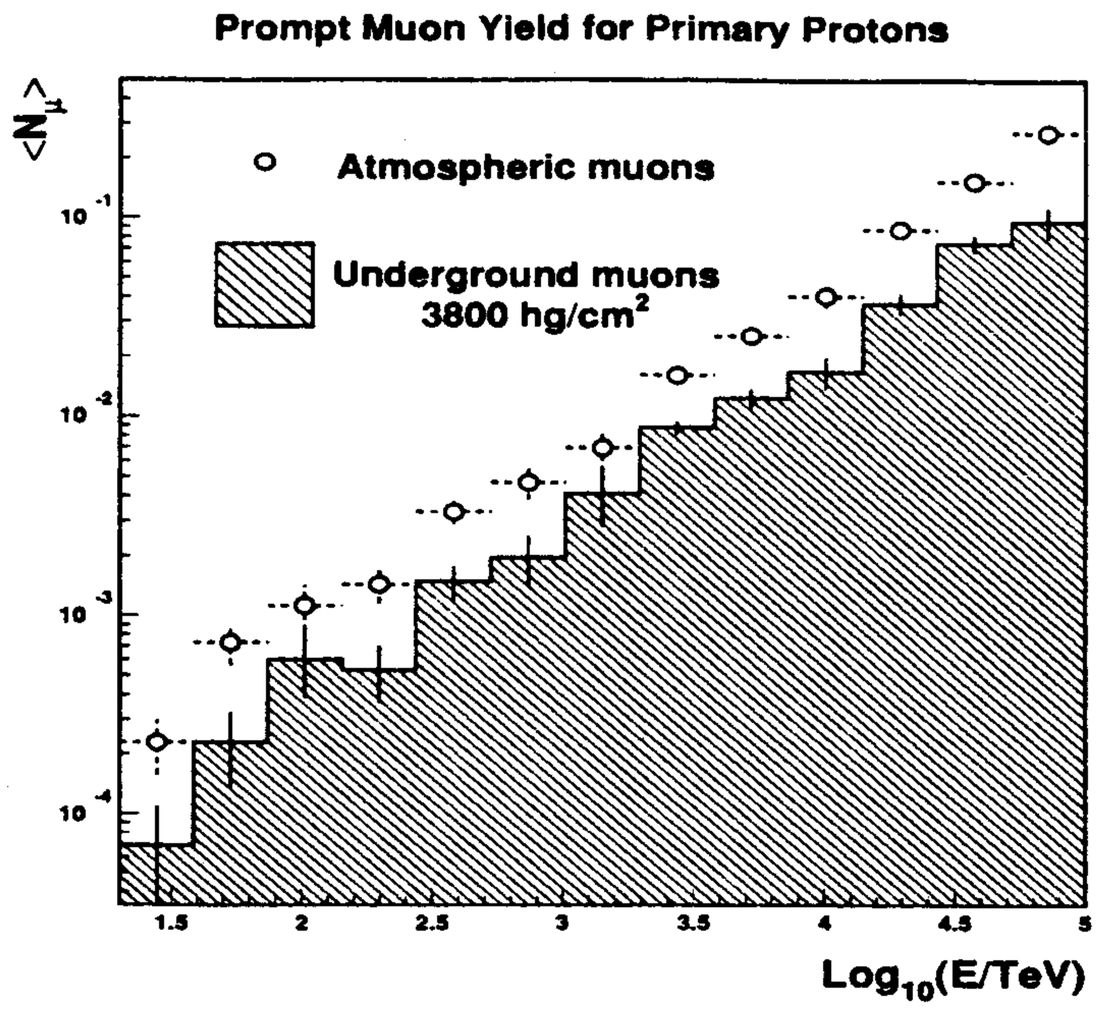

Figure 11: Average prompt muon yield as a function of energy for primary Protons.

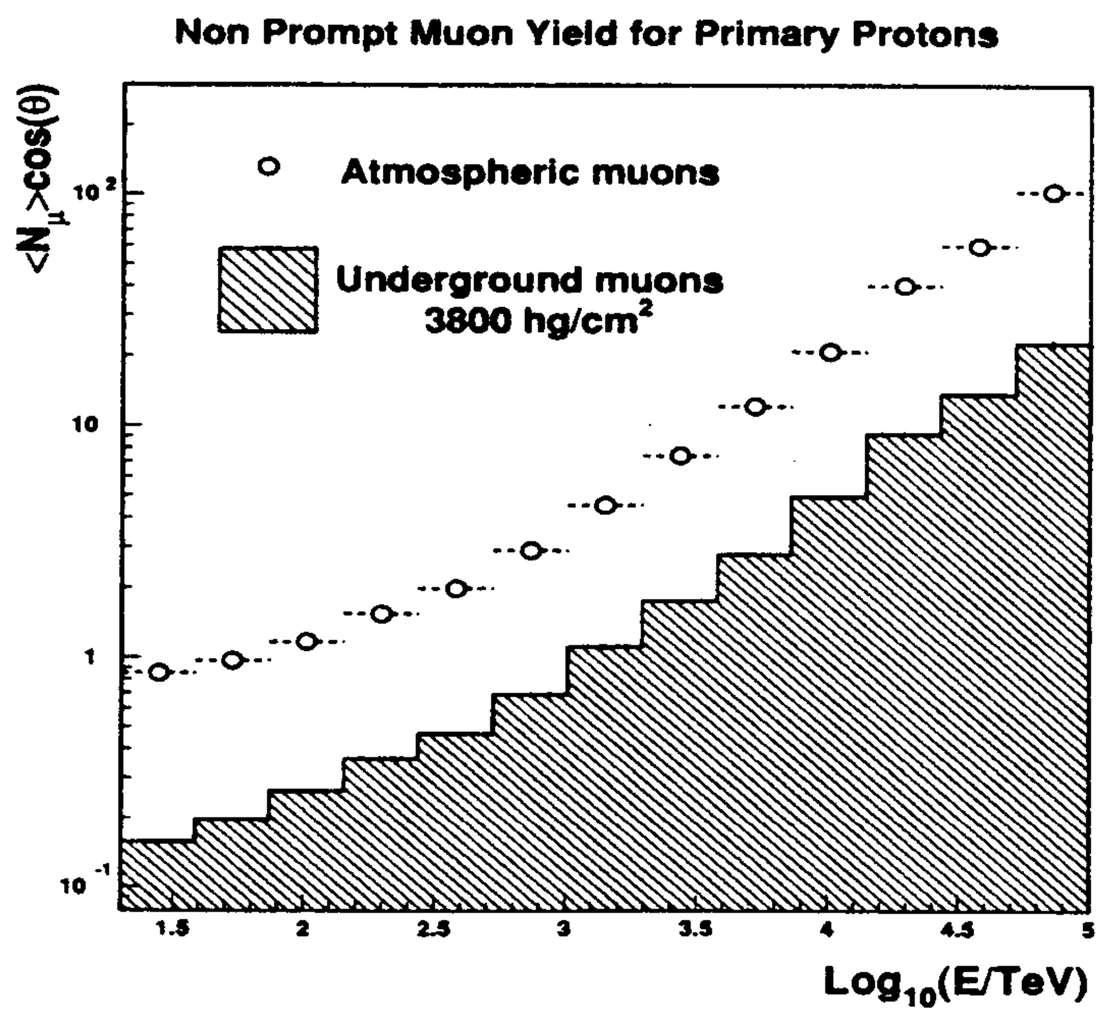

Figure 12: Average non–prompt muon yield, referred to the vertical direction, as a function of energy for primary Protons.

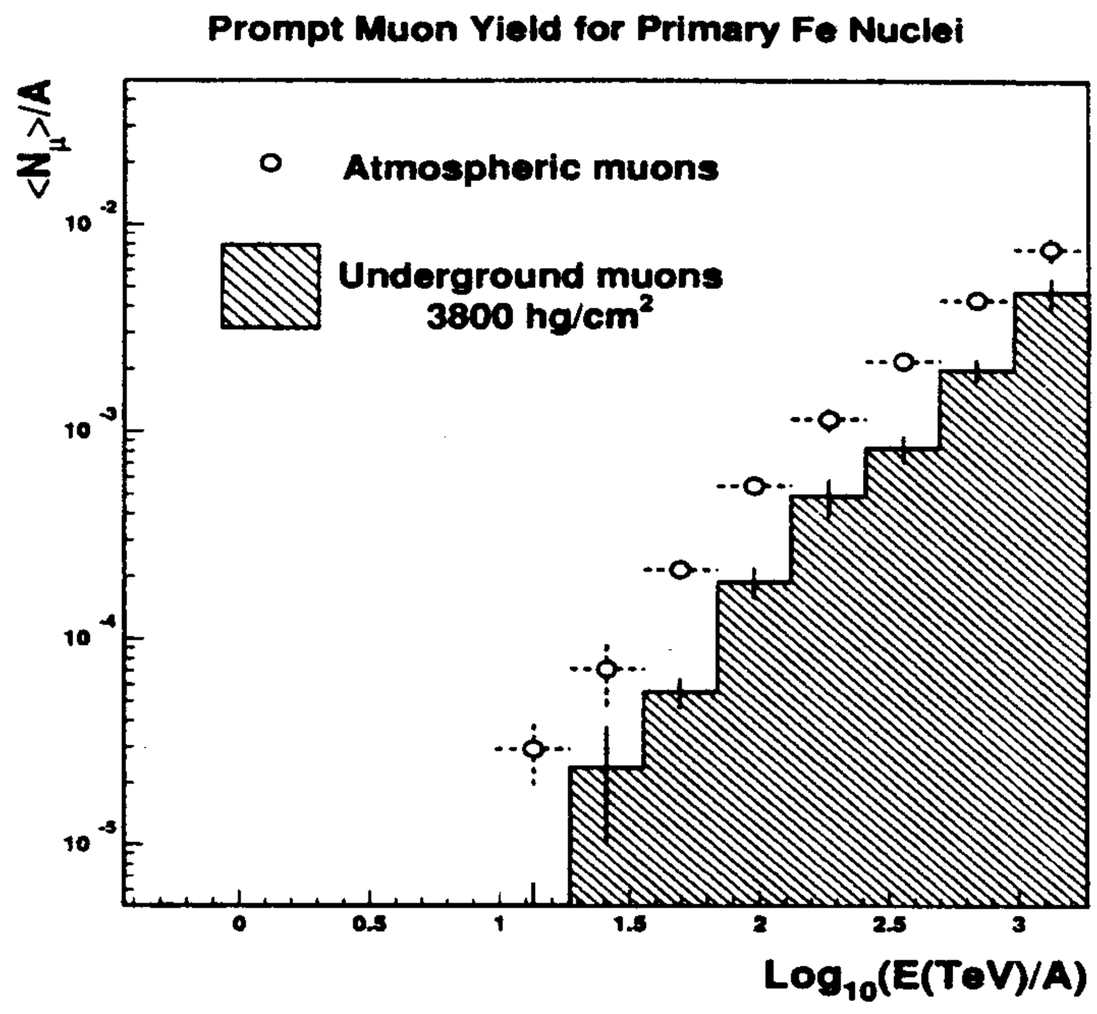

Figure 13: Average prompt muon yield per nucleon as a function of energy per nucleon for primary Fe nuclei.

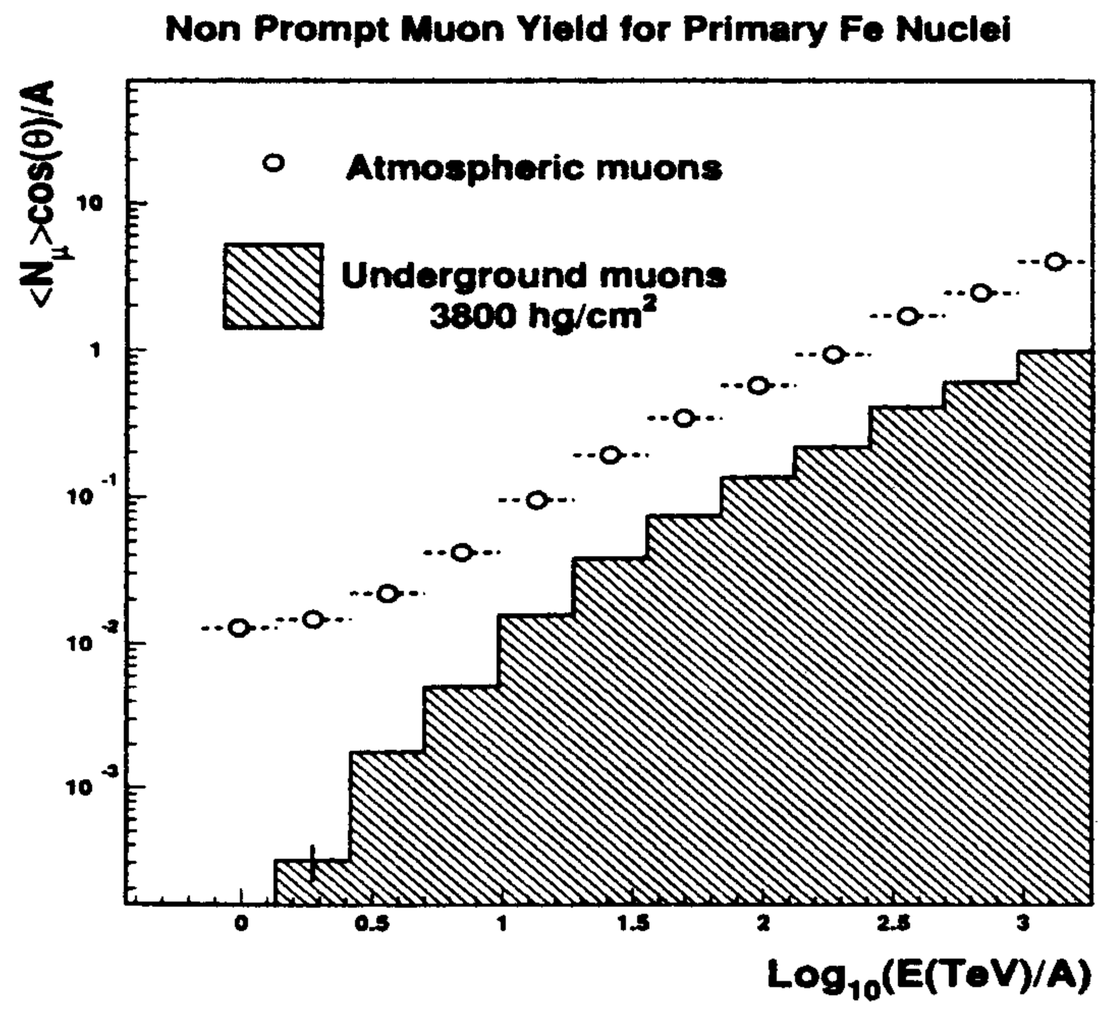

Figure 14: Average non–prompt muon yield per nucleon, referred to the vertical direction, as a function of energy per nucleon for primary Fe nuclei.

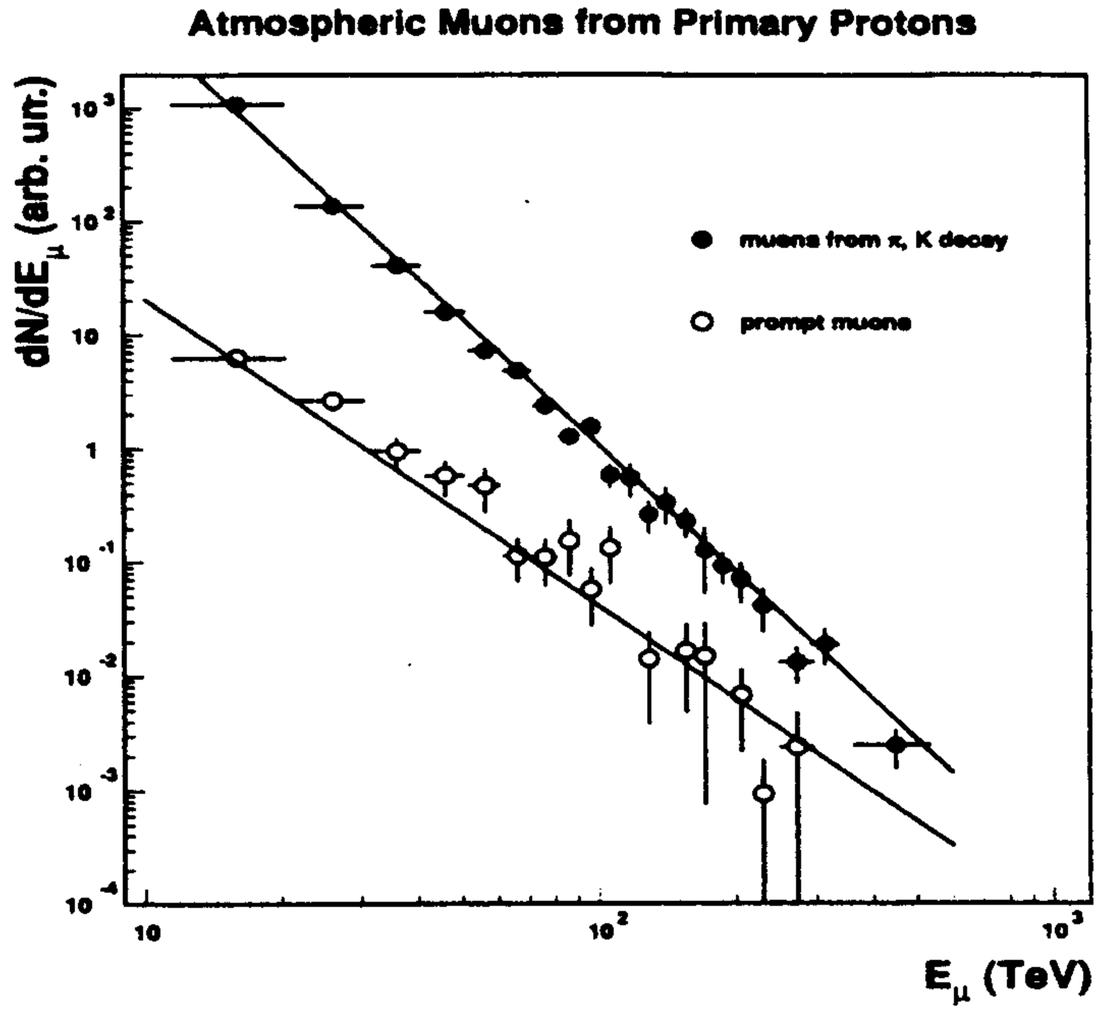

Figure 15: Energy spectra of atmospheric muons from primary protons. The continuous lines are simple power law fits with spectral index 3.7 and 2.7 for the non–prompt and the prompt component respectively.

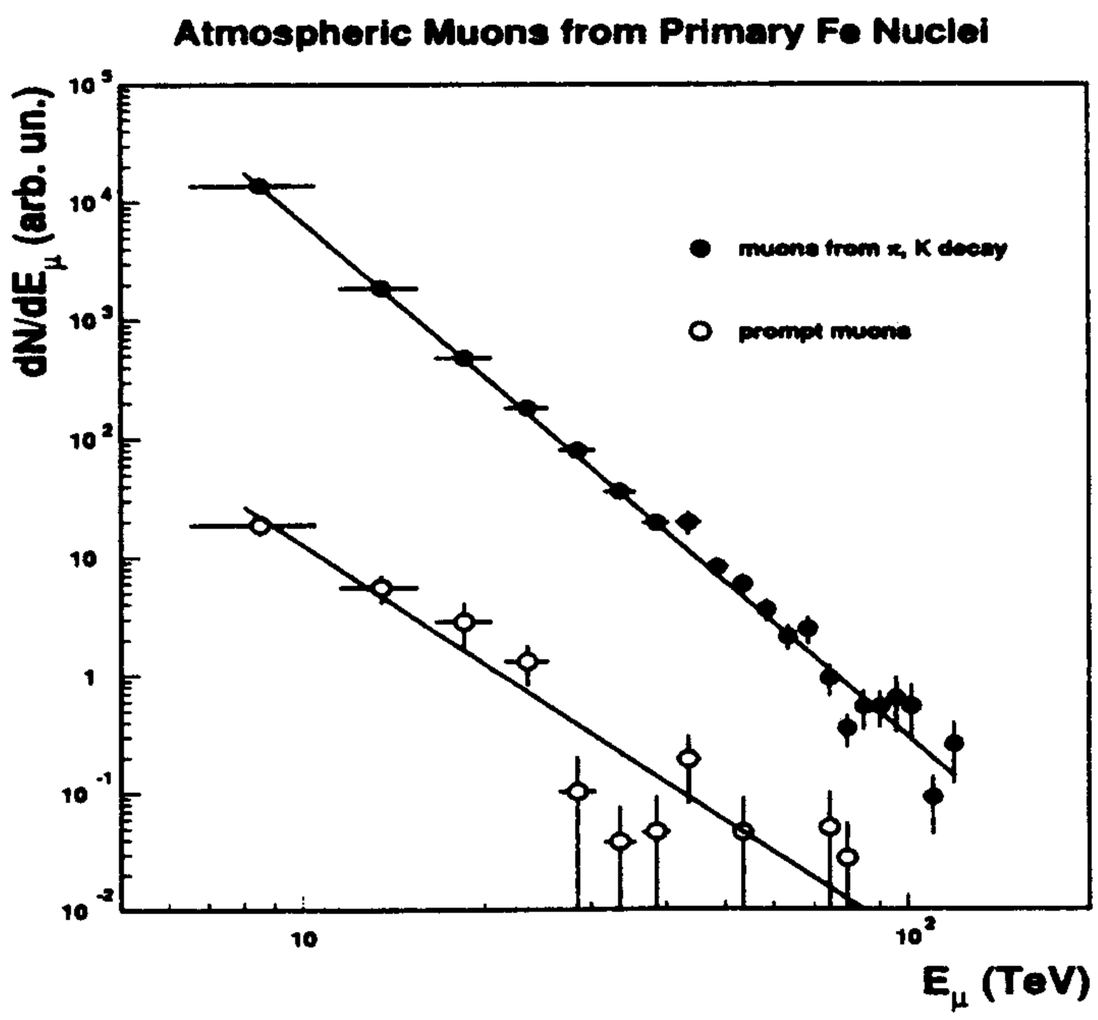

Figure 16: Energy spectra of atmospheric muons from primary Fe nuclei. The continuous lines are simple power law fits with spectral index 3.7 and 2.7 for the non–prompt and the prompt component respectively.

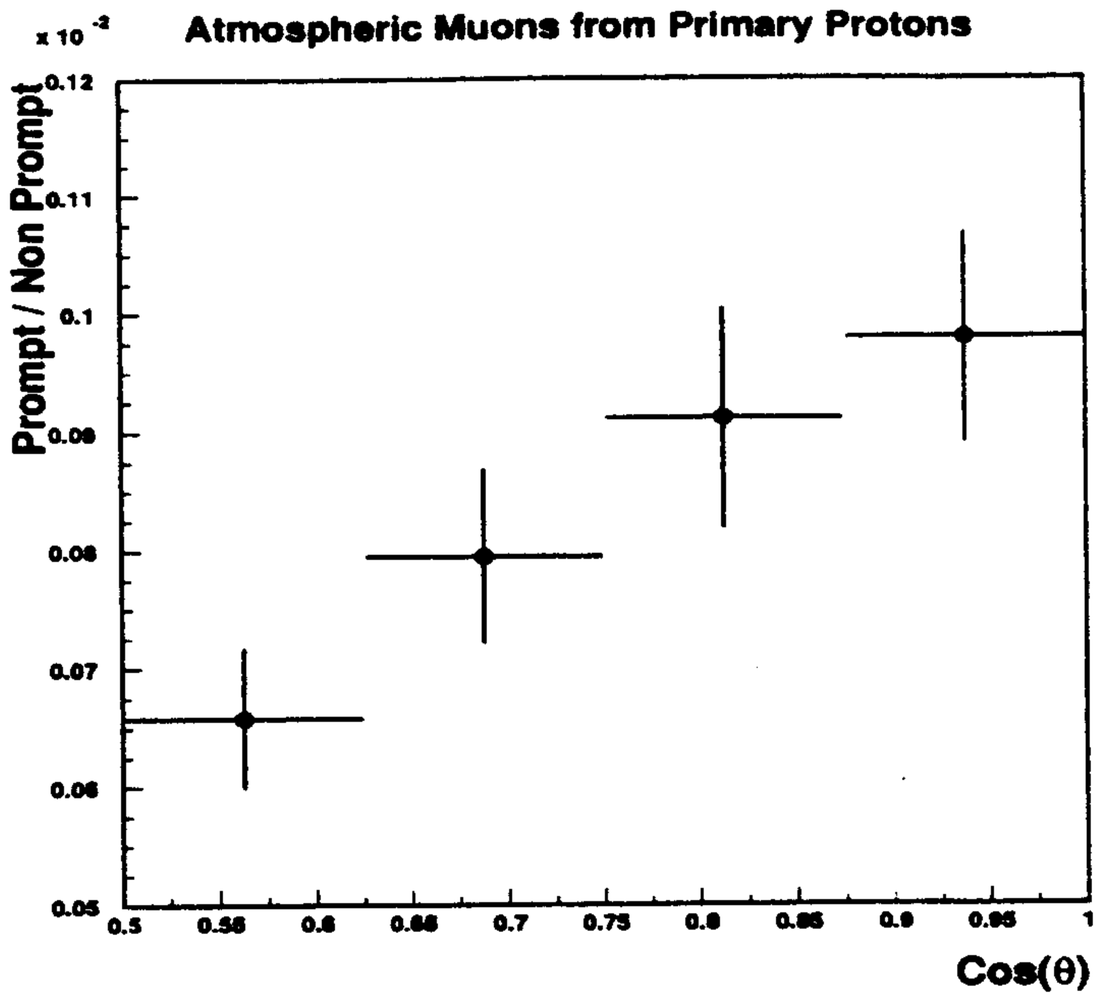

Figure 17: Prompt/non–prompt ratio for atmospheric muons from primary protons as a function of the cosine of the zenith angle.

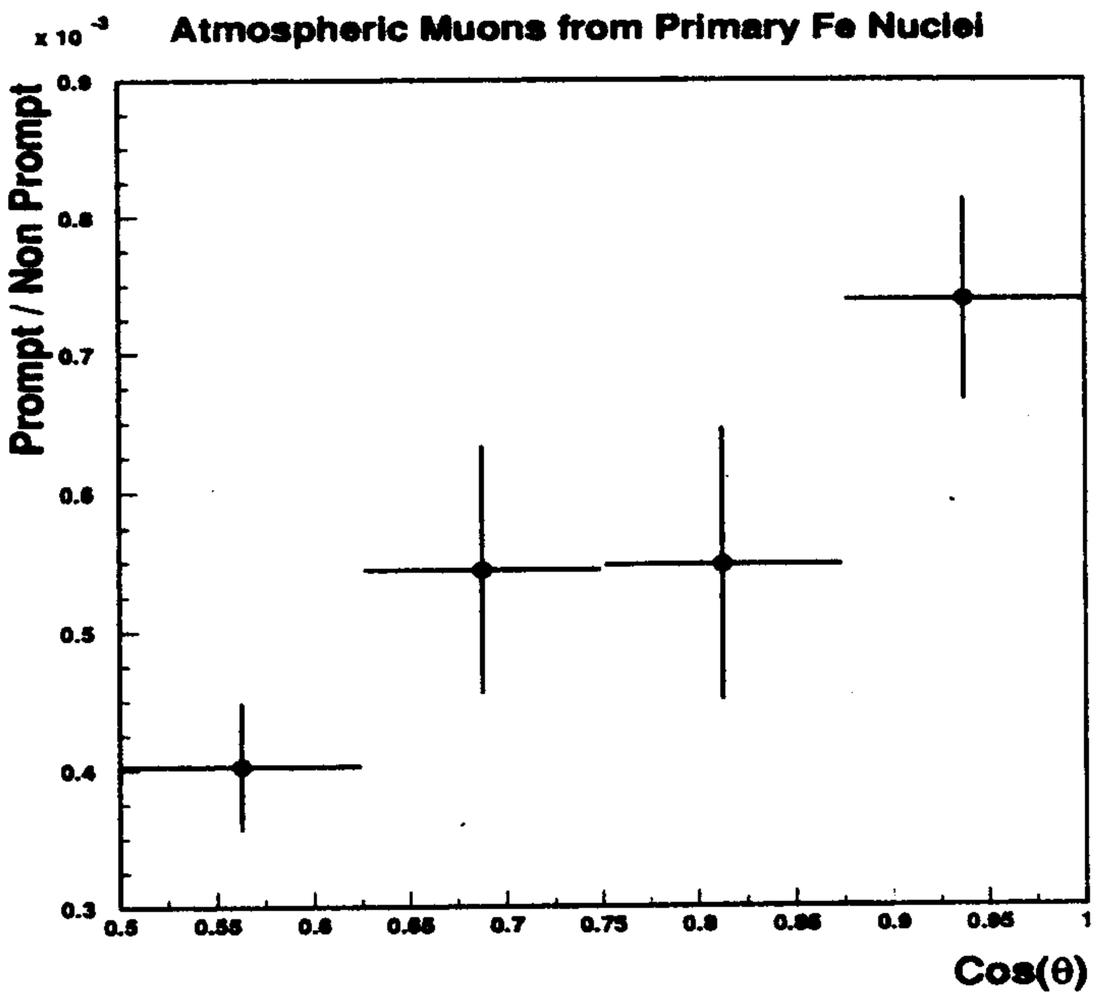

Figure 18: Prompt/non–prompt ratio for atmospheric muons from primary Fe nuclei as a function of the cosine of the zenith angle.

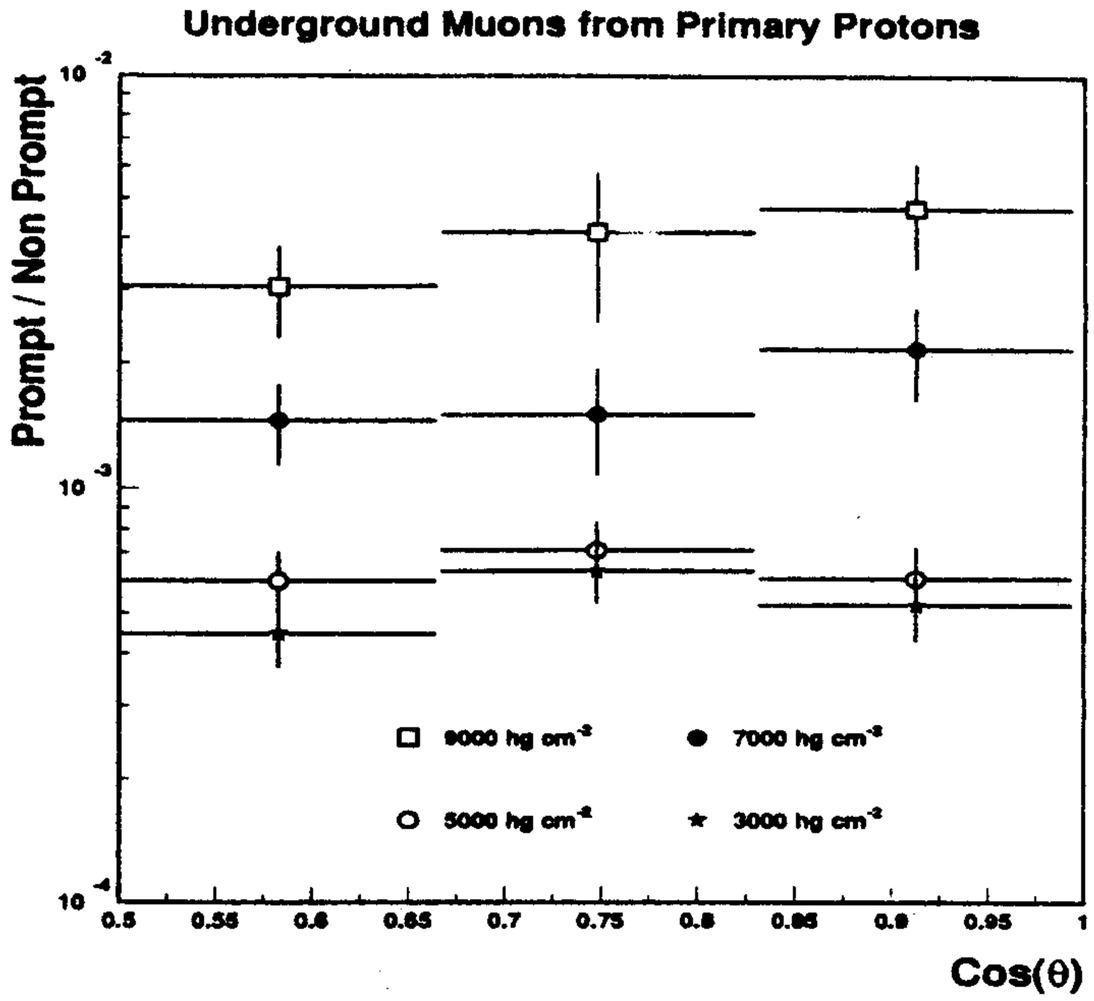

Figure 19: Prompt/non–prompt ratio for underground muons, at different depths, from primary protons as a function of the cosine of the zenith angle.

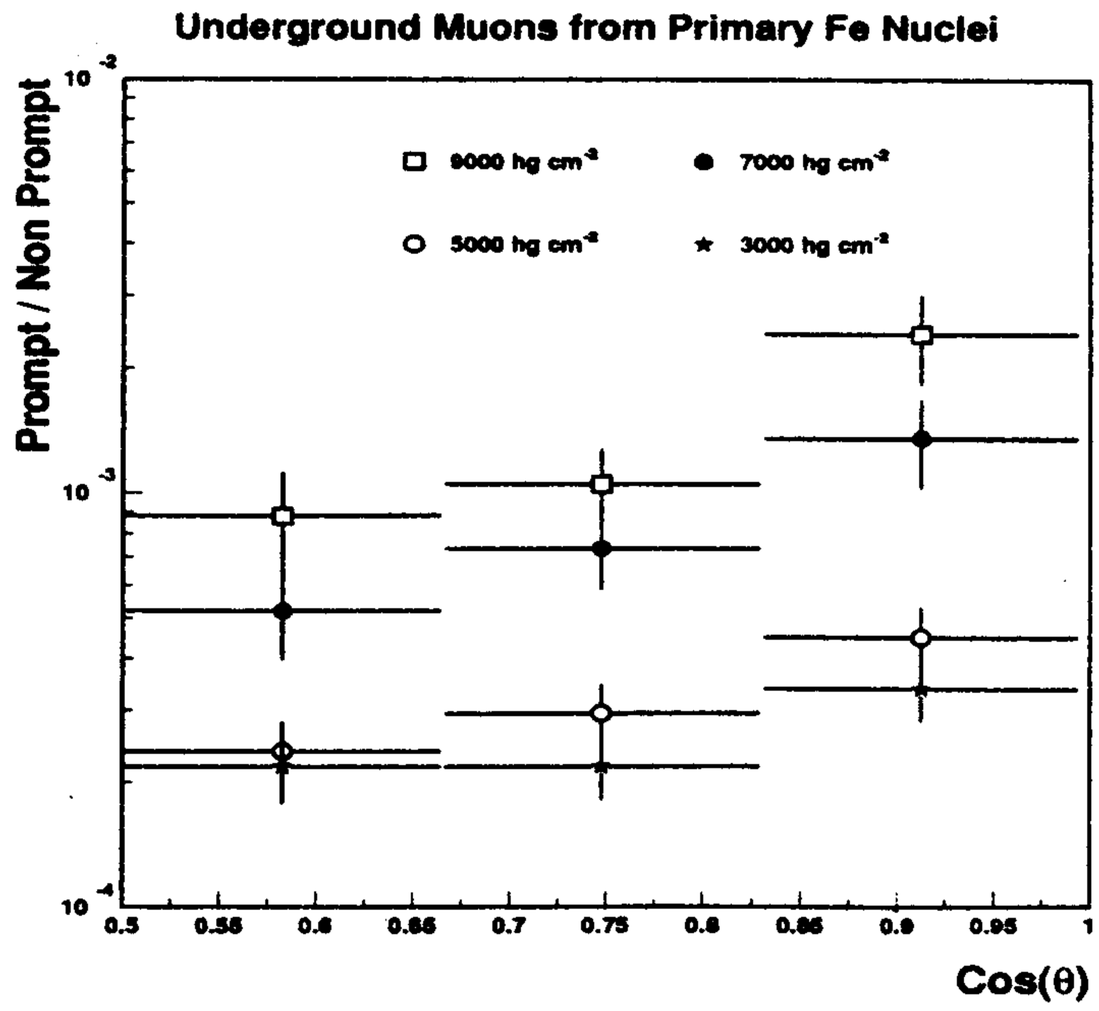

Figure 20: Prompt/non–prompt ratio for underground muons, at different depths, from primary Fe nuclei as a function of the cosine of the zenith angle.

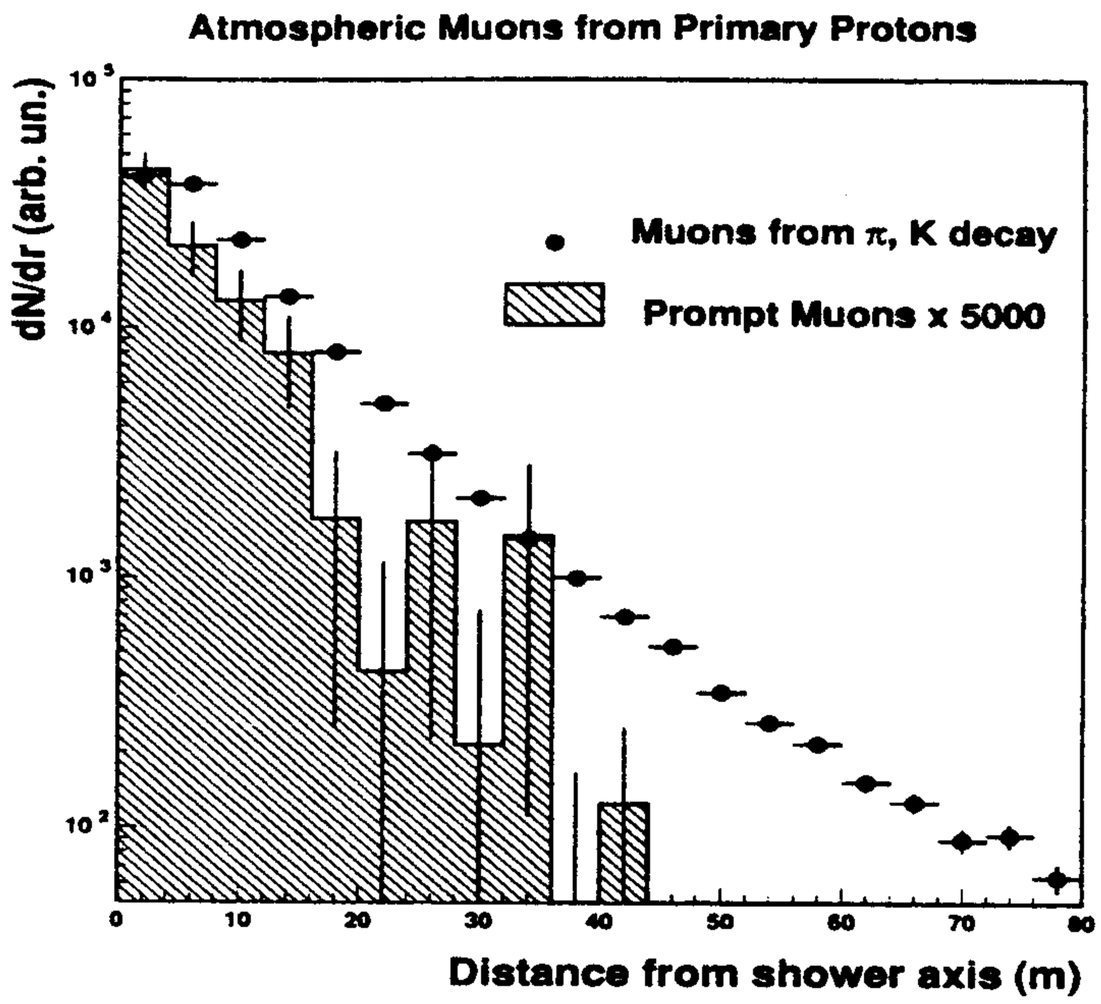

Figure 21: Distribution of the distance from shower axis (lateral distribution function) for non–prompt ($< R_\mu > = 10.66 \pm 0.01$ m) and prompt muons ($< R_\mu > = 7.8 \pm 0.2$ m) in atmosphere at 2000 m a.s.l. in the case of primary protons. We remind that our selection requires $E_\mu \geq 1$ TeV.

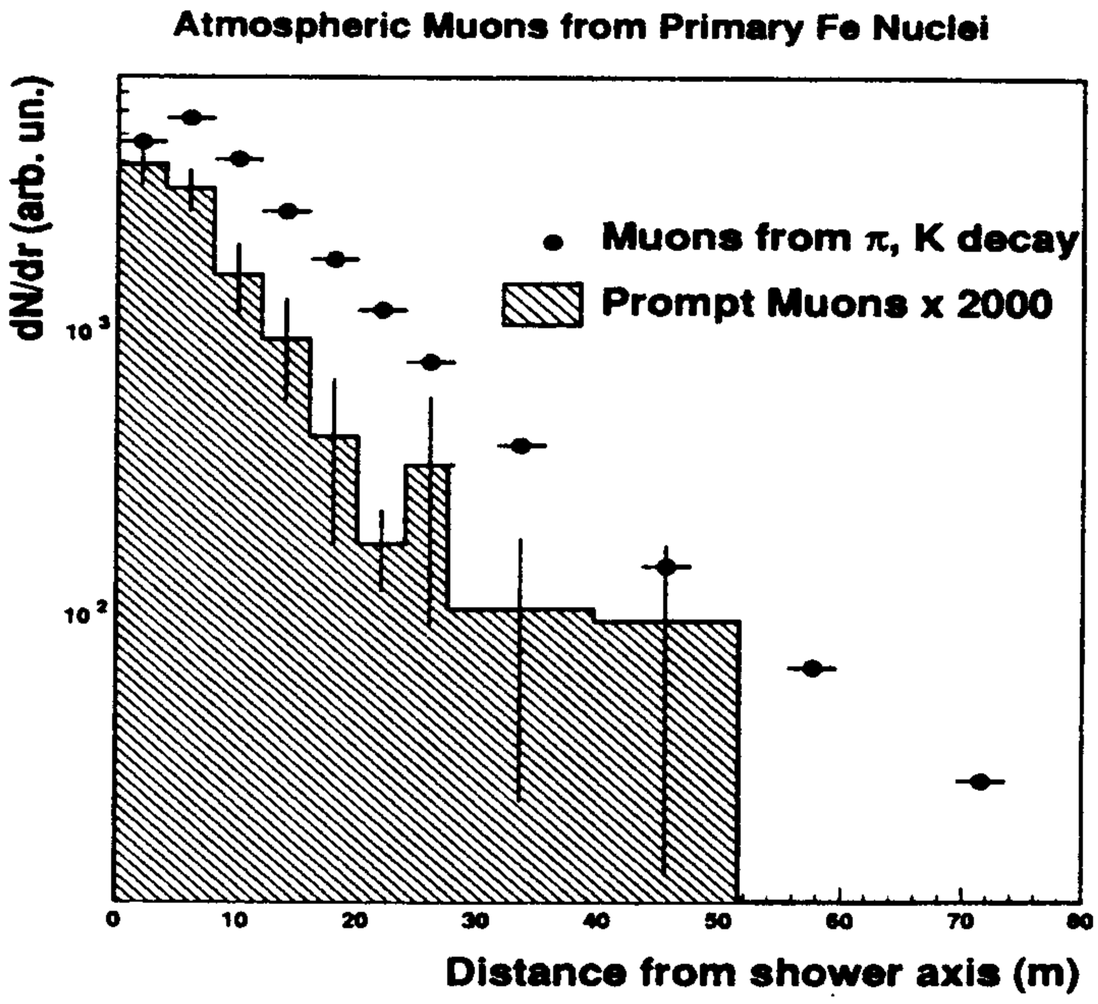

Figure 22: Distribution of the distance from shower axis (lateral distribution function) for non–prompt ($< R_\mu > = 11.76 \pm 0.01$ m) and prompt muons ($< R_\mu > = 9.8 \pm 0.4$ m) in atmosphere at 2000 m a.s.l. in the case of primary Fe nuclei. We remind that our selection requires $E_\mu \geq 1$ TeV.